The strength of SMAD1/5 activity determines the mode of stem cell division in the developing spinal cord

Gwenvael Le Dréau, Murielle Saade, Irene Gutiérrez-Vallejo, and Elisa Martí

Instituto de Biología Molecular de Barcelona, Consejo Superior de Investigaciones Científicas, Parc Científic de Barcelona, Barcelona 08028, Spain

The different modes of stem cell division are tightly regulated to balance growth and differentiation during organ development and homeostasis. However, the mechanisms controlling such events are not fully understood. We have developed markers that provide the single cell resolution necessary to identify the three modes of division occurring in a developing nervous system: self-expanding, self-renewing, and self-consuming. Characterizing these three modes of division during interneuron generation in the developing chick spinal cord, we demonstrated that they correlate to different levels of activity of the canonical bone morphogenetic protein effectors SMAD1/5. Functional in vivo experiments showed that the premature neuronal differentiation and changes in cell cycle parameters caused by SMAD1/5 inhibition were preceded by a reduction of self-expanding divisions in favor of self-consuming divisions. Conversely, SMAD1/5 gain of function promoted self-expanding divisions. Together, these results lead us to propose that the strength of SMAD1/5 activity dictates the mode of stem cell division during spinal interneuron generation.

Introduction

The production of appropriate numbers and types of cells to form a functional central nervous system (CNS) requires a finely tuned balance between the different modes of divisions that neural stem and progenitor cells undergo (Lui et al., 2011; Franco and Müller, 2013). Three distinct modes of divisions occur during vertebrate CNS development: self-expanding (symmetric proliferative [PP]) divisions ensure the expansion of the progenitor pool by generating two daughter cells with identical progenitor potential, self-renewing (asymmetric [PN]) divisions generate one daughter cell with a developmental potential indistinguishable from that of the parental cell and another with a more restricted potential, and self-consuming (symmetric terminal neurogenic [NN]) divisions generate two cells committed to differentiation, thereby depleting the progenitor pool (Götz and Huttner, 2005; Lui et al., 2011; Franco and Müller, 2013). The balance between these modes of stem cell division is also at play during adult neurogenesis in order not to disrupt tissue homeostasis (Suh et al., 2009; Göritz and Frisén, 2012). Given the therapeutic potential of stem cell manipulations in regenerative medicine, it is important to understand the mechanisms regulating these modes of stem cell division.

The intense research over recent years has defined some of the intrinsic mechanisms that govern the mode of division in the developing nervous system. In *Drosophila melanogaster* neuroblasts, particular attention has been paid to the contribution of centrosome asymmetry, spindle orientation, and the inheritance of apical membrane domains (Yu et al., 2006; Gonzalez, 2007; Rebollo et al., 2007). Although not fully understood, the picture emerging suggests that some of the intrinsic mechanisms controlling the mode of division in the developing vertebrate nervous system may reflect similar features (Morin et al., 2007; Ghosh et al., 2008; Marthiens and ffrench-Constant, 2009; Wang et al., 2009; Lesage et al., 2010; Shitamukai et al., 2011; Das and Storey, 2012). However, these decisions are likely to be primarily dictated by extrinsic signals.

Various extrinsic factors have been reported to affect neural stem cell behavior (Fuentealba et al., 2012; Tiberi et al., 2012; Franco and Müller, 2013). However, whether these factors affect

Correspondence to Elisa Martí: emgbmc@ibmb.csic.es; or Gwenvael Le Dréau: gldbmc@ibmb.csic.es

Abbreviations used in this paper: BMP, bone morphogenetic protein; BRE, BMP-responsive element; CNS, central nervous system; GBS, Gli binding site; hpe, hour postelectroporation; hpf, hour postfertilization; MZ, mantle zone; VZ, ventricular zone.

© 2014 Le Dréau et al. This article is distributed under the terms of an Attribution–Noncommercial–Share Alike–No Mirror Sites license for the first six months after the publication date (see http://www.rupress.org/terms). After six months it is available under a Creative Commons License (Attribution–Noncommercial–Share Alike 3.0 Unported license, as described at http://creativecommons.org/licenses/by-nc-sa/3.0/).

The Rockefeller University Press $30.00
J. Cell Biol. Vol. 204 No. 4 591–605
www.jcb.org/cgi/doi/10.1083/jcb.201307031

stem cell proliferation by regulating cell cycle entry, exit, or speed (Salomoni and Calegari, 2010) or whether they directly instruct the mode of stem cell division remains elusive. Additionally, the importance of a particular extrinsic factor appears to depend on the context and to be both stage and area specific (Falk and Sommer, 2009).

To search for the signals controlling the modes of stem cell division in the embryonic CNS, we have recently obtained the single cell resolution necessary for the in vivo identification of the three modes of stem cell division (PP, PN, and NN) within the developing chick spinal cord (Saade et al., 2013). This methodology, which is based on the pTis21:RFP and pSox2:GFP reporters, which are specifically activated during neuron- and progenitor-generating divisions, respectively, allowed us to establish that Sonic Hedgehog directly influences the mode of division of motor neuron progenitors by favoring PP divisions at the expense of PN and NN divisions (Saade et al., 2013). Interestingly, the spatial–temporal dynamics of Sonic Hedgehog signaling suggested that within the spinal cord, the requirement of this pathway in regulating the modes of division is restricted to motor neuron progenitors, leaving unresolved the nature of the extrinsic signal, which plays an equivalent role later during the generation of spinal interneurons.

Here, we characterized in vivo the modes of divisions used by interneuron progenitors within the developing chick spinal cord. We examined, based on its spatial–temporal activity, the putative involvement of the canonical bone morphogenetic protein (BMP) pathway in the control of those division modes. We found that at the mitotic phase, high, intermediate, and low levels of activity of the canonical BMP effectors SMAD1/5 correlate with PP, PN, and NN divisions, respectively. Furthermore, in vivo loss- and gain-of-function experiments showed that high levels of SMAD1/5 signaling promote PP divisions, whereas a reduction in SMAD1/5 activity forces spinal progenitors to prematurely switch to NN divisions. These results led us to conclude that an endogenous gradient of SMAD1/5 activity dictates the mode of division of spinal interneuron progenitors.

Results

PP, PN, and NN divisions co-occur during spinal cord neurogenesis

From the onset of neurogenesis within the developing vertebrate CNS, neural progenitors can use three distinct modes of divisions: self-expanding (symmetric proliferative [PP]), self-renewing (asymmetric [PN]), and self-consuming (NN; Götz and Huttner, 2005; Lui et al., 2011). We recently described a methodology based on the activity of the pTis21:RFP and pSox2:GFP reporters, which allows to unequivocally identify and distinguish these three modes of divisions in the chick spinal cord in vivo (Saade et al., 2013). Whereas the pTis21:RFP reporter distinguishes pTis21:RFP$^+$ neuron-generating divisions (PN and NN) from pTis21:RFP$^-$ ones (PP), the pSox2:GFP reporter discriminates pSox2:GFP$^+$ progenitor-generating (PP + PN) divisions from pSox2:GFP$^-$ (NN) ones (Saade et al., 2013).

Herein, we used this methodology to characterize the modes of divisions that neural progenitors undergo during the production of interneurons, which emerge along the whole dorsal–ventral axis, except the pMN domain, from stage HH18 (72 h postfertilization [hpf] and 30/36 somites; see Le Dréau et al., 2012). Coelectroporating in ovo these two reporters into HH14 chick embryos (54 hpf and 22 somites) revealed at 24 h postelectroporation (hpe; 24 hpe = ~HH18) that the three populations of electroporated cells (GFP$^+$/RFP$^-$, GFP$^+$/RFP$^+$, and GFP$^-$/RFP$^+$) are observed along the dorsal–ventral axis of the developing spinal cord (Fig. 1, A and B). To quantify the proportions of the three modes of divisions, we confined our analysis to 16 hpe on mitotic (pH3$^+$) electroporated cells to ensure that we only tracked cycling progenitor cells. Quantification at different time points demonstrated the progressive increase in the proportion of PN (GFP$^+$/RFP$^+$) divisions at the expense of PP (GFP$^+$/RFP$^-$) followed by the appearance of NN (GFP$^-$/RFP$^+$) divisions around 70 hpf (Fig. 1 C). Interestingly, we observed a sharp drop in the proportion of PP (GFP$^+$/RFP$^-$) divisions between 64 and 74 hpf (from 88 ± 11 to 32 ± 8; Fig. 1 C), as recently reported for the single pMN domain (Saade et al., 2013). Thus, the three different modes of neural progenitor division all occur along the dorsal–ventral axis during spinal interneuron generation (Fig. 1 D).

To pinpoint which extrinsic signal could be controlling the modes of progenitor divisions during spinal interneuron generation, we assessed the endogenous activity of the Sonic Hedgehog and canonical Wnt and BMP pathways, which are all known to play key roles in stem cell maintenance (Morrison and Spradling, 2008), and during early spinal cord development (Ulloa and Briscoe, 2007; Le Dréau and Martí, 2012). Electroporation of a Wnt-responsive reporter (TOP:H2B-RFP) together with a control H2B-GFP vector at HH14 showed at 24 hpe that the canonical Wnt activity was restricted to the most dorsal part of the neural tube (Fig. 1 E). Conversely, electroporation of a Gli binding site (GBS):H2B-GFP reporter serving as a readout of Sonic Hedgehog signaling showed its activity to be restricted to the ventral part of the neural tube (Fig. 1 F). In contrast, the canonical BMP pathway appeared to be active along the dorsal–ventral axis of the developing spinal cord, as demonstrated by the activity of the BMP-responsive element (BRE):EGFP reporter (Fig. 1 G). The BRE:EGFP reporter activity was high in the dorsal-most part of the neural tube, reflecting the early role of BMPs during neural patterning (Le Dréau et al., 2012; Tozer et al., 2013). In addition, scattered GFP$^+$ cells were detected along the whole dorsal–ventral axis, at the time of interneuron neurogenesis (Le Dréau et al., 2012). These results suggested that the canonical BMP pathway could be controlling the distinct modes of neural progenitor division during spinal interneuron generation.

The distinct modes of division are correlated to different levels of endogenous canonical BMP activity

Thus, we next examined whether the different modes of divisions were correlated in the developing spinal cord with distinct levels of endogenous activity of SMAD1/5/8, the effectors of the

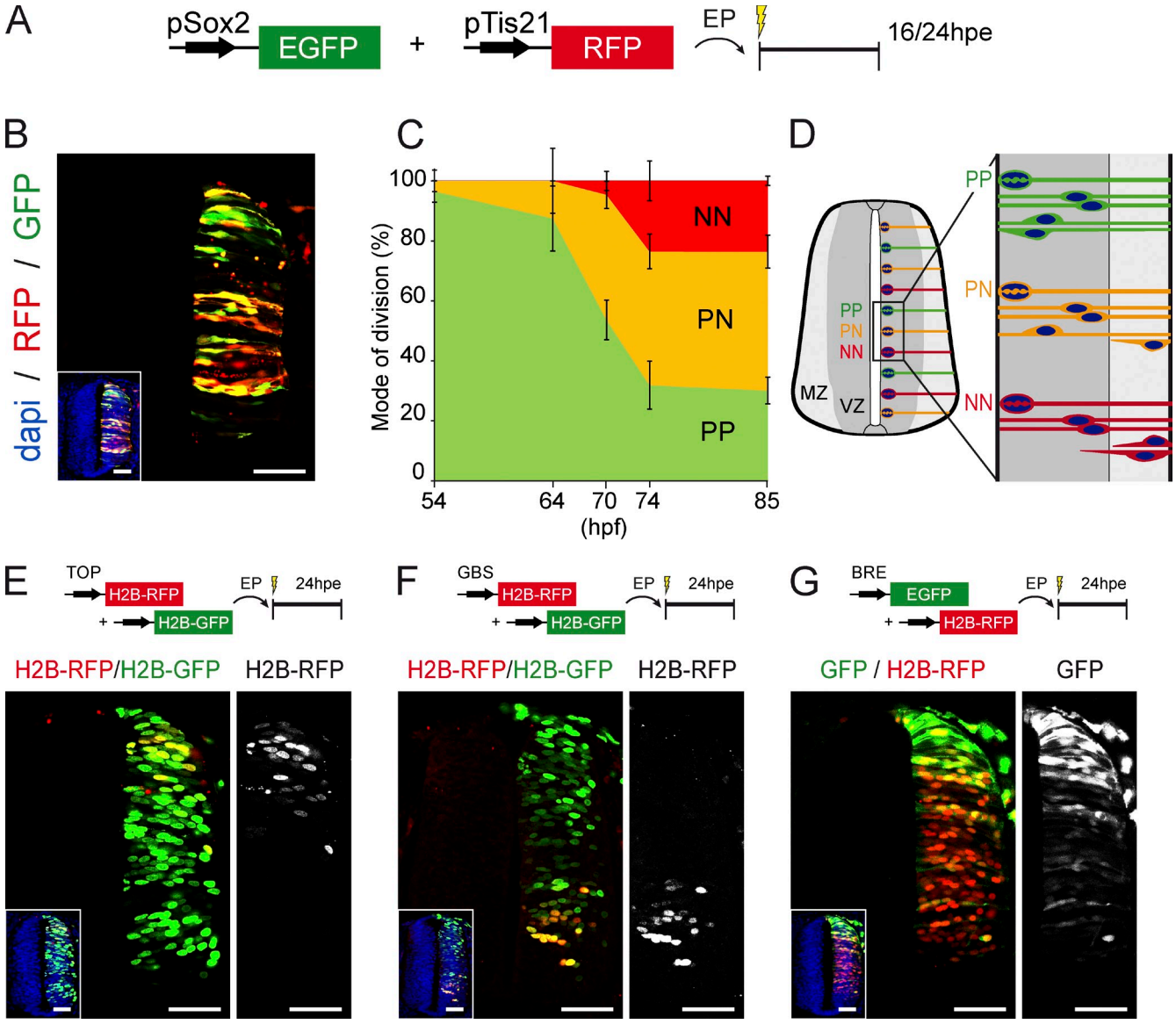

Figure 1. **PP, PN, and NN divisions co-occur during spinal cord neurogenesis.** (A) In ovo electroporation (EP) of the pTis21:RFP and pSox2:GFP reporters allows us to identify and discriminate the populations and divisions of PP, PN, and NN progenitors within the developing chick spinal cord. (B) Representative neural tube section obtained at 24 hpe of HH14 embryos, showing GFP$^+$;RFP$^-$ (PP), GFP$^+$;RFP$^+$ (PN), and GFP$^-$;RFP$^+$ (NN) cells in response to differential activities of the pTis21:RFP and pSox2:GFP reporters. The inset shows the neural tube morphology, with nuclei stained with DAPI. (C) The proportions of PP, PN, and NN divisions were assessed at 16 hpe at different developmental points, with a combination of the pSox2:EGFP and pTis21:RFP reporters and pH3 staining to reveal mitoses. Error bars show means ± SEM. (D) Illustration of the three modes of divisions occurring along the dorsal–ventral axis of a developing spinal cord during interneuron neurogenesis. (E–G) Representative neural tube sections obtained 24 h after coelectroporation of HH14 embryos with combinations of the TOP:H2B-RFP (E), GBS:H2B-RFP (F), or BRE:EGFP (G) with their respective controls. The insets show the neural tube morphology, with nuclei stained with DAPI. The right images show the signal observed in response to the specific activity of the corresponding reporter. Bars, 50 µM.

canonical BMP pathway (Massagué et al., 2005). To this end, we took advantage of an anti–phospho-SMAD1/5/8 (pS158) antibody to locate the active forms of SMAD1/5/8 in dividing neural progenitors. As previously reported in different areas of the developing vertebrate CNS (Müller et al., 2005; Alarcón et al., 2009), pS158 immunoreactivity was particularly strong in the mitotic nuclei lining the neural tube lumen (Fig. 2, A and B). This immunoreactivity was observed not only in all the nuclei stained with the mitotic marker pH3 (Fig. 2 A) but also in the nuclei displaying diffuse lamin B1 immunoreactivity, indicative of the lamin solubilization that occurs before chromosomal condensation and nuclear envelope breakdown (Fig. 2 B).

We quantified the pS158 immunoreactivity in mitotic nuclei 24 hpe and related this to the modes of division using the pSox2:GFP and pTis21:RFP reporters (Fig. 2, C–H). There was a 34% increase in nuclear pS158 intensity in pSox2$^+$ dividing cells as compared with pSox2$^-$ mitoses (mean nuclear pS158 intensity of 128 ± 3.5 in pSox2$^+$ vs. 95 ± 2.5 in pSox2$^-$; $P < 0.001$; Fig. 2, C and D), indicating that SMAD1/5/8 activity was weaker during NN divisions than during progenitor-generating (PP + PN) divisions. Conversely, the nuclear pS158 intensity in pTis21$^+$ divisions was significantly weaker than in pTis21$^-$ nuclei (mean nuclear pS158 intensity of 96 ± 4.1 in pTis21$^+$ vs. 115 ± 5.2 in pTis21$^-$; $P < 0.05$; Fig. 2, E and F), indicating

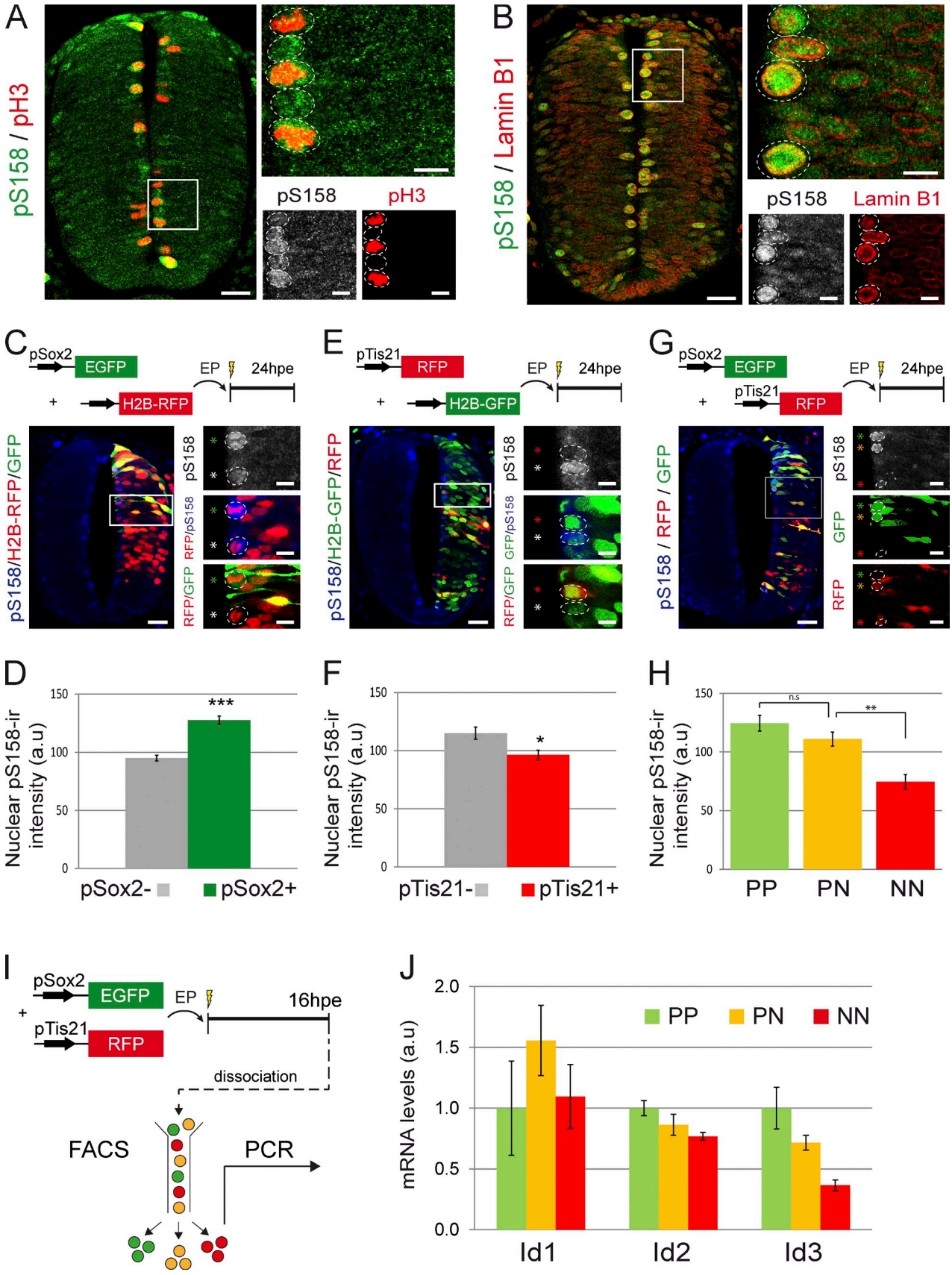

Figure 2. **Quantification of endogenous SMAD1/5 activity and *Id* gene expression in function of the mode of division.** (A and B) Representative sections of HH18 neural tubes stained for the active form of SMAD1/5/8 (pS158) and pH3 (A) or lamin B1 (B). (C–H) Analysis of the endogenous SMAD1/5/8 activity in the distinct modes of divisions. Neural tube sections were stained for pS158 24 hpe of HH14 embryos with a combination of the pSox2:EGFP

stronger SMAD1/5/8 activity during PP divisions than in neurogenic (PN + NN) divisions. Finally, quantification of the nuclear pS158 staining after coelectroporation with both reporters confirmed that SMAD1/5/8 activity was significantly weaker in neural progenitors undergoing NN divisions than in those undergoing progenitor-generating (PP + PN) divisions (mean nuclear pS158 intensity of 75 ± 6.2 for NN vs. 111 ± 6.0 for PN [$P < 0.01$] and 124 ± 6.7 for PP vs. 111 ± 6.0 for PN [$P > 0.05$]; Fig. 2, G and H). Therefore, the variations in the endogenous level of SMAD1/5/8 activity were directly correlated with neural progenitor divisions, with the highest levels associated with PP divisions and the lowest levels with NN divisions.

To support this idea, we investigated whether target genes of the canonical BMP pathway showed changes in expression levels in correlation with the distinct modes of divisions. Genes of the *Id* (*Inhibitor of DNA binding*) family are considered as prototypical direct targets of the canonical BMP pathway (Hollnagel et al., 1999; Korchynskyi and ten Dijke, 2002; Ying et al., 2003). Within the developing spinal cord, *Id1*, *Id2*, and *Id3* might indeed represent bona fide direct targets of the canonical BMP pathway, as their expression levels were, respectively, increased and decreased in response to BMP signaling gain and loss of function (Fig. S1). Therefore, we next analyzed by semiquantitative PCR their expression levels within PP, PN, and NN cell subpopulations that had been previously purified by FACS 16 h after coelectroporation of the pSox2:EGFP and pTis21:RFP reporters (Fig. 2 I). Both *Id2* and *Id3* transcripts presented expression levels higher in PP than in PN than in NN subpopulations (Fig. 2 J). Thus, the regulation of two out of three likely direct target genes of the canonical BMP pathway presented a pattern similar to the one obtained after pS158 quantification. Altogether, these results strongly support the idea that the distinct modes of progenitor division are correlated to different levels of endogenous canonical BMP activity during spinal interneuron neurogenesis.

SMAD1/5 activity is required to maintain self-expanding divisions and to restrain neurogenic divisions

Next, we determined whether SMAD activity influences the modes of division adopted by spinal progenitors. Because we previously demonstrated that SMAD8 is required only for the generation of the most dorsal population of interneurons (dI1; Le Dréau et al., 2012), we focused our attention on the activity of SMAD1 and SMAD5.

We analyzed the consequences of SMAD1/5 inhibition on the modes of division after electroporation of shRNA constructs targeting chick *Smad1* or *Smad5* (sh-S1 and sh-S5, respectively; see Materials and methods). We first performed coelectroporation experiments in which the pTis21:RFP reporter was combined with the sh-S1/5 or control vectors together with an H2B-GFP–expressing vector to follow electroporated cells (Fig. 3 A). 24 hpe, we observed a significant increase in the percentage of $pTis21^+$ dividing progenitors in the absence of SMAD1/5 activity compared with control (percentages of $H2B\text{-}GFP^+;pH3^+;pTis21^+$ cells were 66 ± 2 for control, 86 ± 3 for sh-S1, and 85 ± 3 for sh-S5; $P < 0.01$; Fig. 3 B), indicating that reduced SMAD1/5 activity increased the proportion of neuron-generating divisions (PN + NN).

Similar experiments performed with the pSox2:EGFP reporter revealed that the proportion of $pSox2^+$ dividing progenitors was significantly lower than in the controls when this reporter was coelectroporated with sh-S1/5 constructs (percentages of $H2B\text{-}RFP^+;pH3^+;pSox2^+$ cells were 81 ± 2 for control, 58 ± 5 for sh-S1, and 65 ± 3 for sh-S5; $P < 0.01$; Fig. 3, C and D). These results indicated that *Smad1/5* knockdown reduced the proportion of progenitor-generating divisions (PP + PN). Coelectroporation of a constitutively active SMAD5 mutant (SMAD5-SD) together with the sh-S5 construct reverted both the proportions of $pTis21^+$ divisions and $pSox2^+$ divisions at the levels obtained by control electroporation (Fig. S2, A and B), thereby ensuring of the specificity of the phenotype.

Considering that PP and NN divisions correspond to $pTis21^-$ and $pSox2^-$ divisions, respectively (see Materials and methods; Saade et al., 2013), we extracted the proportion of PN divisions as %PN = 100 − (%PP + %NN). This revealed that *Smad1/5* knockdown induced an increase in NN divisions of approximately twofold (percentages of NN were 19 ± 2 for control, 42 ± 5 for sh-S1, and 36 ± 3 for sh-S5; $P < 0.01$; Fig. 3 E) and an equivalent approximate twofold reduction in PP divisions (percentages of PP were 34 ± 2 for control, 14 ± 3 for sh-S1, and 15 ± 3 for sh-S5; $P < 0.01$: Fig. 3 E), without affecting PN divisions (percentages of PN were 47 ± 4 for control, 44 ± 8 for sh-S1, and 50 ± 6 for sh-S5: Fig. 3 E). Moreover, inhibiting SMAD1/5 activity by overexpressing Somitabun, a *Smad5* mutant acting as a dominant negative to SMAD1/5/8 (Hild et al., 1999), produced similar results (Figs. 3 F and S2, C and D). Interestingly, increasing concentrations of Somitabun resulted in a gradual increase in the proportion of NN divisions concomitant with a gradual decrease in the proportion of PP divisions (Fig. 3 F). Together, these results established that the mode of division adopted by spinal progenitors depends on the level of SMAD1/5 activity and that high SMAD1/5 activity is required to maintain PP divisions and restrain premature NN divisions (Fig. 3 G).

We next performed the converse experiment by analyzing the consequences of SMAD1/5 overactivation on the modes of divisions. Constitutively active forms of SMAD1 or SMAD5 (SMAD1-SD and SMAD5-SD, respectively; see Le Dréau et al.,

and the control H2B-RFP vector (C), the pTis21:RFP and the control H2B-GFP vector (E), or both pSox2:EGFP and pTis21:RFP reporters (G). The intensity of the mean nuclear pS158 staining was measured in $pSox2^-$ and $pSox2^+$ mitoses (D), in $pTis21^-$ and $pTis21^+$ mitoses (F), or in mitotic $GFP^+;RFP^-$ (PP), $GFP^+;RFP^+$ (PN), and $GFP^-;RFP^+$ (NN) progenitors (H). (I) Illustration of the methodology used to analyze the levels of Id1/2/3 transcripts expressed by the PP, PN, and NN subpopulations. (J) Semiquantitative PCR analysis of the mRNA levels of Id1, Id2, and Id3 transcripts expressed by $GFP^+;RFP^-$ (PP), $GFP^+;RFP^+$ (PN), and $GFP^-;RFP^+$ (NN) cells. a.u., arbitrary unit; EP, electroporation. Error bars show means ± SEM. *, $P < 0.05$; **, $P < 0.01$; ***, $P < 0.001$. Bars: (main images) 25 µM; (insets) 10 µM. The higher magnification pictures originate from the corresponding insets. The dotted lines delineate nuclei. The asterisks show the cells of interest.

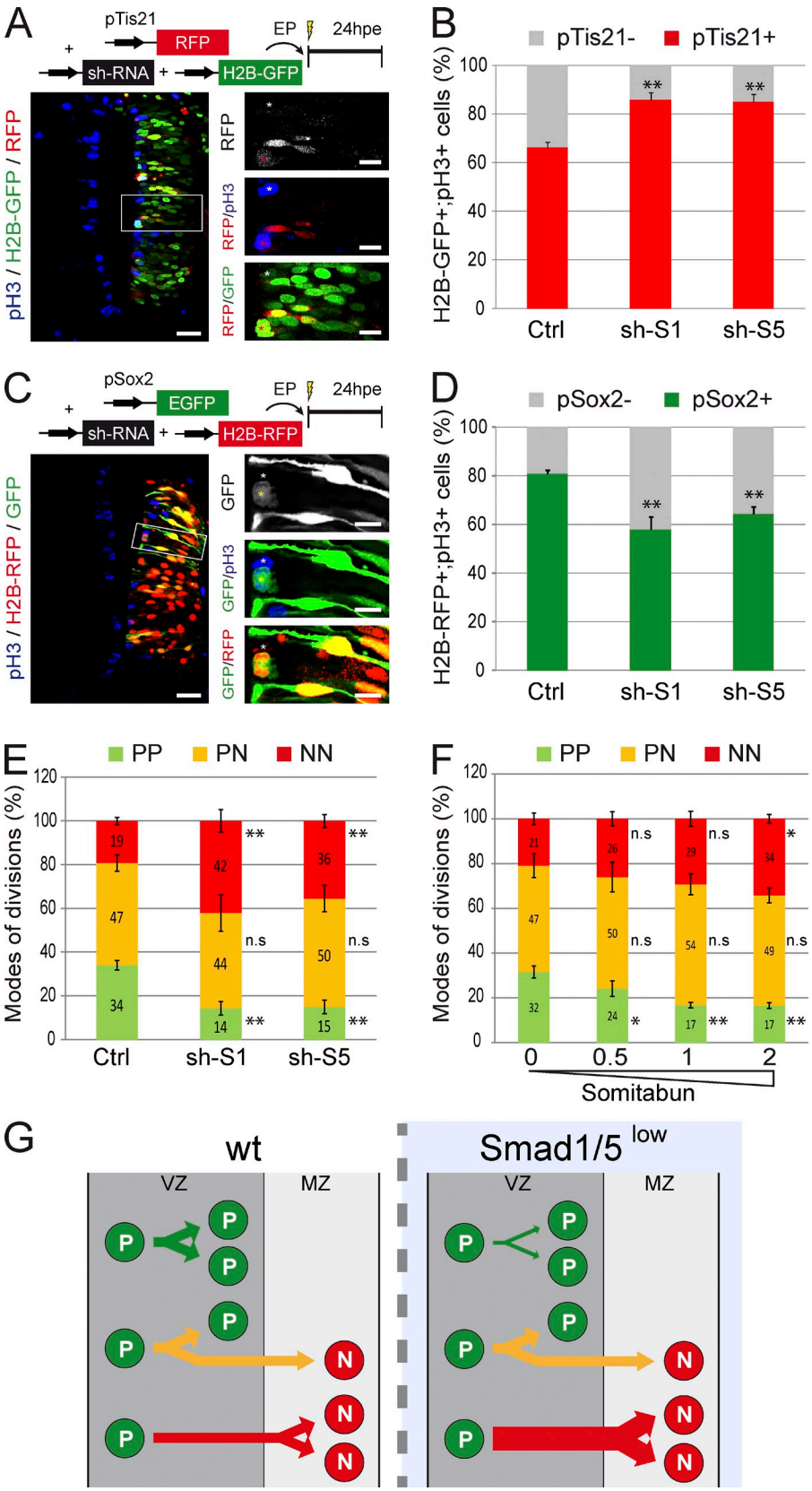

Figure 3. **SMAD1/5 activity is required to maintain self-expanding divisions.** (A–D) Analysis of neurogenic (PN + NN) and progenitor-generating (PP + PN) divisions in vivo. Transverse sections were stained for pH3 to identify mitotic progenitors at 24 hpe of HH14 embryos with control (Ctrl) or *Smad1/5* shRNA (sh-S1 and sh-S5) constructs, together with the pTis21:RFP reporter and a control H2B-GFP vector (A) or with the pSox2:GFP reporter and control H2B-RFP vector (C). The higher magnification pictures originate from the corresponding insets. Proportions of mitotic electroporated (H2B-GFP$^+$;pH3$^+$ [B] or H2B-RFP$^+$;pH3$^+$ [D]) progenitors based on the activity of the pTis21:RFP (B) or pSox2:EGFP (D) reporters. (E) Proportions of the three modes of divisions (PP, PN, and NN) obtained 24 hpe with control or *Smad1/5* shRNA vectors (sh-S1 or sh-S5). These percentages were deduced from the earlier results, considering that the %PP = %pTis21$^-$, %NN = %pSox2$^-$, and %PN = 100 − (%PP + %NN). (F) Proportions of the modes of divisions obtained 24 hpe with 0, 0.5, 1, or 2 µg/µl Somitabun. (G) Illustration of the increase in NN divisions obtained at the expense of PP divisions after SMAD1/5 inhibition in spinal neural progenitors. EP, electroporation; wt, wild type. Error bars show means ± SEM. *, P < 0.05; **, P < 0.01. Bars: (main images) 25 µM; (insets) 10 µM.

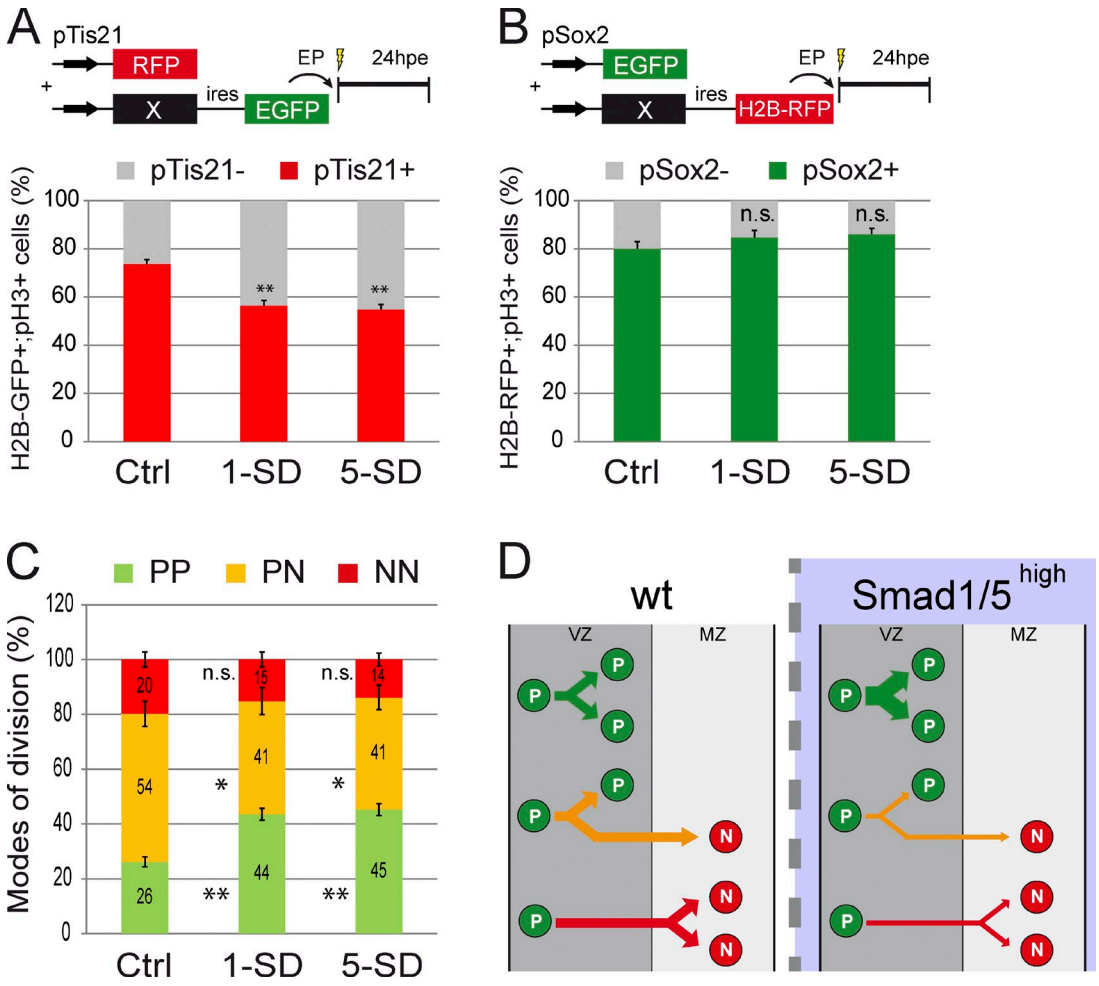

Figure 4. **Strong SMAD1/5 activity promotes PP divisions at the expense of PN and NN divisions.** (A and B) Proportions of mitotic electroporated progenitors (H2B-GFP$^+$;pH3$^+$ [A] or H2B-RFP$^+$;pH3$^+$ [B]) based on the activity of the pTis21:RFP (A) or pSox2:EGFP (B) reporters at 24 h after coelectroporation of HH14 embryos with control (Ctrl), SMAD1-SD (1-SD), or SMAD5-SD (5-SD). (C) Percentages of the three modes of divisions (PP, PN, and NN) obtained at 24 hpe with the constructs indicated and deduced from earlier results, considering that %PP = %pTis21$^-$, %NN = %pSox2$^-$, and %PN = 100 − (%PP + %NN). (D) Illustration of the increase in PP divisions obtained at the expense of PN and NN divisions after SMAD1/5 overactivation in spinal progenitors. EP, electroporation; wt, wild type. Error bars show means ± SEM. *, $P < 0.05$; **, $P < 0.01$.

2012) were electroporated in combination with the pTis21:RFP or pSox2:GFP reporters. SMAD1/5-SD significantly decreased the proportion of pTis21$^+$ divisions (percentages of H2B-GFP$^+$;pH3$^+$;pTis21$^+$ cells were 74 ± 2 for control, 57 ± 2 for SMAD1-SD, and 55 ± 2 for SMAD5-SD; $P < 0.01$; Fig. 4 A). The percentage of pSox2$^+$ dividing cells augmented only slightly after SMAD1/5 overactivation (percentages of H2B-RFP$^+$;pH3$^+$;pSox2$^+$ cells were 80 ± 3 for control, 85 ± 3 for SMAD1-SD, and 86 ± 2 for SMAD5-SD: Fig. 4 B). The percentages of the three modes of divisions deduced from these data suggested that SMAD1/5 overactivation increased PP divisions (percentages of PP were 26 ± 1 for control, 44 ± 2 for SMAD1-SD, and 45 ± 2 for SMAD5-SD; $P < 0.01$; Fig. 4 C) at the expense of PN (percentages of PN were 54 ± 5 for control, 41 ± 5 for SMAD1-SD, and 41 ± 4 for SMAD5-SD; $P < 0.05$; Fig. 4 C) and NN divisions (percentages of NN were 20 ± 3 for control, 15 ± 2 for SMAD1-SD, and 14 ± 2 for SMAD5-SD; Fig. 4 C). Thus, high levels of SMAD1/5 activity were sufficient to promote self-expanding divisions (Fig. 4 D).

SMAD1/5 activity is required to maintain spinal progenitor cells

We reasoned that the concomitant decrease in PP and increase in NN divisions, which are caused by SMAD1/5 inhibition should alter the pace of neuronal differentiation. We thus analyzed the time course of neuronal differentiation after interfering with SMAD1/5 activity. The proportion of electroporated cells (H2B-RFP$^+$) differentiated into neurons (HuC/D$^+$) was significantly higher from 24 h after *Smad1/5* knockdown onwards (percentages of H2B-RFP$^+$;HuC/D$^+$ cells at 38 hpe were 31 ± 3 for control, 55 ± 4 for sh-S1, and 54 ± 3 for sh-S5; $P < 0.01$; Figs. 5 A and S3 A), indicating that the loss of SMAD1/5 activity caused the premature differentiation of neural progenitors in a cell-autonomous manner. To confirm this result, we took advantage of the Tubb3enh:EGFP reporter (Bergsland et al., 2011), which contains an EGFP cassette driven by an enhancer of the *β3-tubulin* gene, the expression of which is activated during neuronal differentiation. More H2B-RFP$^+$;GFP$^+$ cells were observed in embryos electroporated

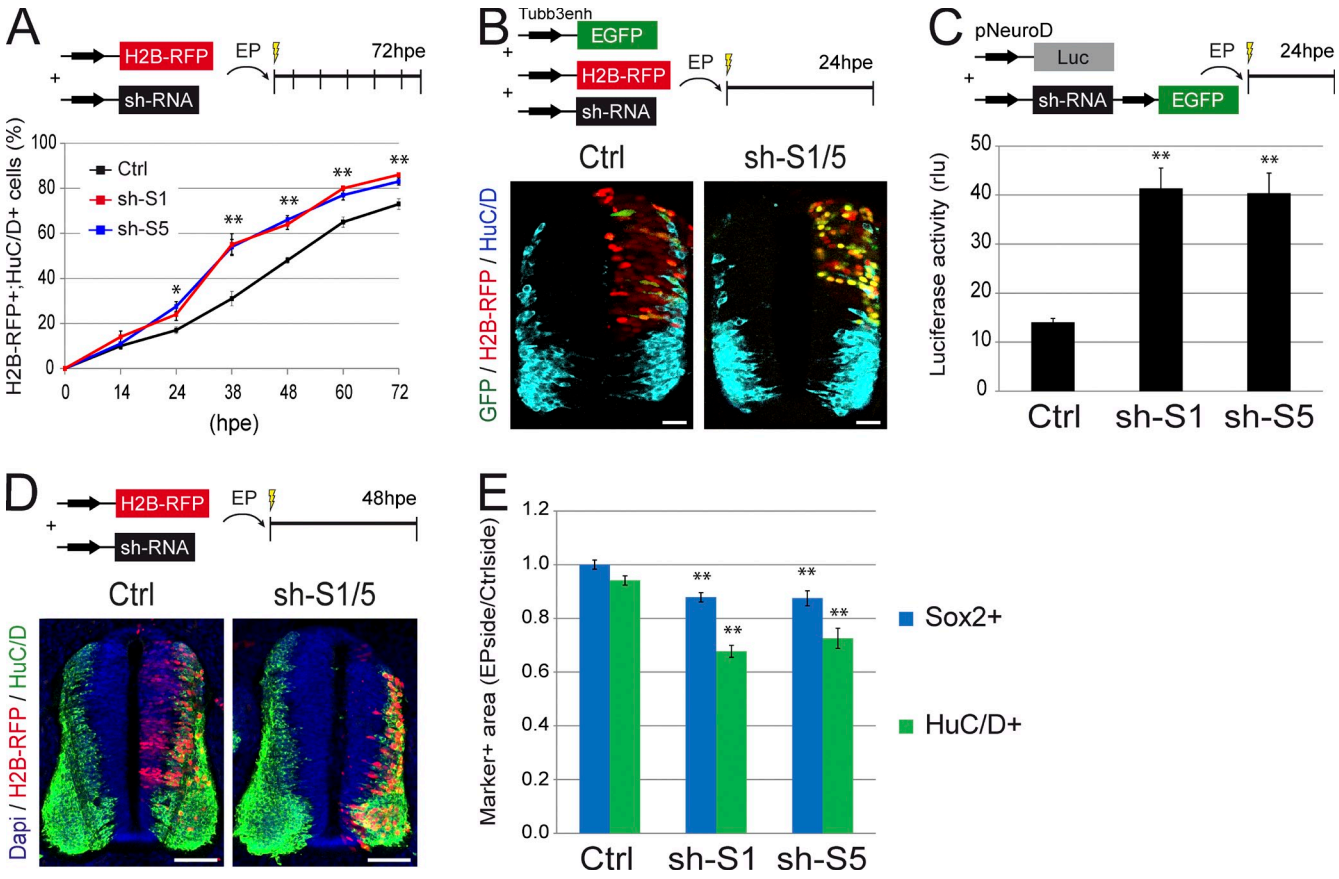

Figure 5. **SMAD1/5 inhibition triggers premature differentiation in a cell-autonomous manner.** (A) Proportions of electroporated cells differentiated into neurons (H2B-RFP$^+$;HuC/D$^+$) obtained after electroporation of HH14 embryos with control (Ctrl) and *Smad1/5* shRNA (sh-S1 and sh-S5) constructs, in sections of neural tubes recovered at the times indicated (hpe). (B) Representative sections stained for HuC/D expression 24 h after coelectroporation with the Tubb3enh: EGFP reporter, the control H2B-RFP vector, and control or *Smad1/5* shRNA (sh-S1/5). (C) Quantification of luciferase activity (expressed in relative luciferase units [rlu]) driven by the pNeuroD reporter at 24 hpe with the *Smad1/5* shRNA (sh-S1 or sh-S5) or control vectors. (D) Representative transverse sections of a chick neural tube at 48 hpe with control or *Smad1/5* shRNA (sh-S1/5). DAPI, HuC/D, and H2B-RFP stain nuclei, differentiating neurons and electroporated cells. (E) Analysis of the ratios of the areas occupied by the VZ (Sox2$^+$) and MZ (HuC/D$^+$) measured for the electroporated side and standardized to their contralateral controls. EP, electroporation. Error bars show means ± SEM. *, $P < 0.05$; **, $P < 0.01$. Bars: (B) 25 µM; (D) 50 µM.

with sh-S1 and sh-S5 than in the controls at 24 hpe (Fig. 5 B). At 24 hpe, *Smad1/5* knockdown had moreover triggered an approximately threefold increase in the activity of a luciferase (Luc) reporter driven by a fragment of the *NeuroD* promoter, a basic helix–loop–helix factor known to activate the panneurogenic differentiation program (pNeuroD:Luc; 14.0 ± 0.8 for control, 41.3 ± 4.2 for sh-S1, and 40.4 ± 4.1 for sh-S5; $P < 0.01$; Fig. 5 C).

At 48 hpe, the proportion of H2B-RFP$^+$;HuC/D$^+$ cells was still higher in sh-S1 and sh-S5 embryos than in control ones (Fig. 5, A and D). We also noticed that fewer HuC/D$^+$ cells were evident in the mantle zone (MZ; the lateral region of the neural tube formed by neurons) after *Smad1/5* knockdown than in the controls (Figs. 5 D and S3 A). This observation was confirmed by measuring the area occupied by the MZ, which showed an ~30% reduction in response to SMAD1/5 knockdown (Figs. 5 E and S3 B). Interestingly, this was associated with an ~15% decrease in the area occupied by the ventricular zone (VZ) containing the Sox2$^+$ progenitors (Figs. 5 E and S3 B).

Loss of SMAD1/5 activity causes a specific shortening of the S phase

Distinct stem cell fates and modes of division have been correlated with variations in the cell cycle kinetics of neural progenitors in the developing cerebral cortex (Dehay and Kennedy, 2007; Salomoni and Calegari, 2010). To test how SMAD1/5 activity influences the cell cycle, we measured the duration of the different cell cycle phases by performing cumulative BrdU experiments (see Materials and methods; Nowakowski et al., 1989). When we assessed the index of BrdU labeling in electroporated cells (H2B-RFP$^+$) located in the VZ at 48 hpe (Fig. 6 A), the fraction of cells in the S phase (indicated by the intercept of the BrdU labeling curve with the *y* axis) was significantly smaller for sh-S1 (0.24) and sh-S5 (0.21) cells than for the controls (0.35: Fig. 6 B). In contrast, the time needed for the BrdU labeling index to reach the plateau (representing the Tc − Ts length) was comparable for control (7.0 h), sh-S1 (7.6 h), and sh-S5 (7.7 h) cells. Similarly, the fraction of cycling cells was nearly identical in control (0.77 ± 0.01) and in sh-S1 (0.74 ± 0.01) and sh-S5 (0.76 ± 0.02) electroporated embryos. These data

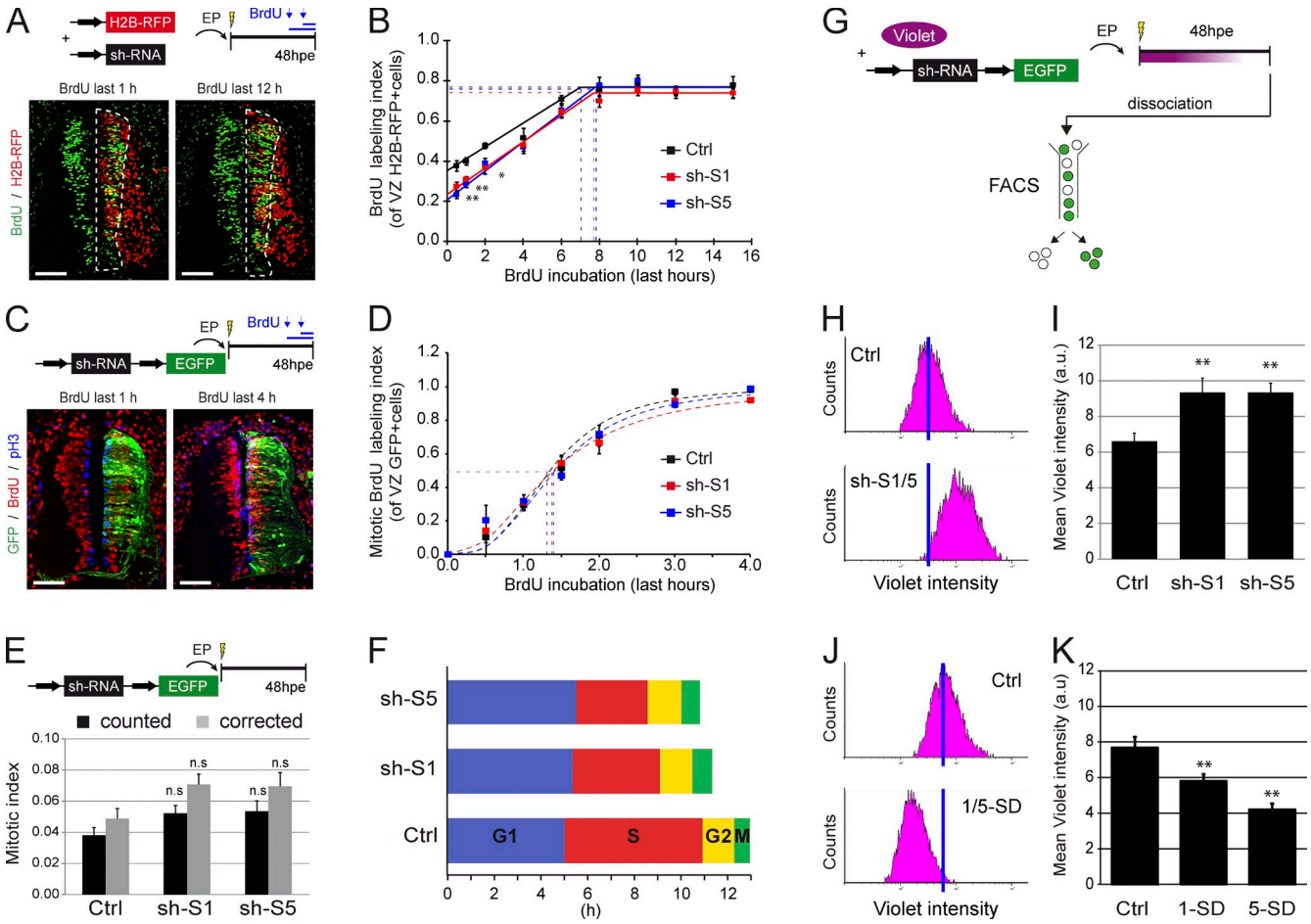

Figure 6. **Loss of SMAD1/5 activity causes a specific shortening of the S phase.** (A) Representative sections of neural tubes at 48 hpe, after incorporation of BrdU in the last 1 and 12 h. BrdU staining was observed in a fraction of the electroporated H2B-RFP$^+$ neural progenitors that were still present in the VZ (dashed lines). (B) BrdU labeling index calculated for neural progenitors electroporated (H2B-RFP$^+$) with control (Ctrl), *Smad1* (sh-S1), or *Smad5* (sh-S5) shRNA vectors. Dashed lines show the growth fraction (*y* axis) and the duration of BrdU incorporation needed to reach the plateau, which represents the ($T_c - T_S$) value (*x* axis). (C) Representative sections showing BrdU staining in a fraction of the mitotic (pH3$^+$) electroporated (GFP$^+$) neural progenitors. (D) Mitotic BrdU labeling index calculated for cells electroporated (GFP$^+$) with control, *Smad1*, or *Smad5* (sh-S5) shRNA vectors. Dashed lines show the duration of the BrdU incorporation needed to label 50% of the cell population (*y* axis), which represents the mean T_{G2} value (*x* axis). (E) Mitotic index calculated for cells electroporated (GFP$^+$) with control, *Smad1* (sh-S1), or *Smad5* (sh-S5) shRNA vectors. Both the mean values obtained from counting and those corrected with respect to differential growth fraction values are given. (F) Graphical representation of the duration of the cell cycle (Tc) and its distinct phases measured for control, *Smad1* (sh-S1), or *Smad5* shRNA (sh-S5) electroporated cells. (G–K) Illustration of the method used to assess neural progenitor divisions in vivo (G), after loss (H and I) or gain of function (J and K) of SMAD1/5 activity. (H and J) Representative pictures of the CellTrace violet intensity measured by flow cytometry in dissociated cells at 48 hpe with the indicated constructs. The blue bars highlight the mean intensity obtained in the control condition. (I and K) Quantification of the mean CellTrace violet intensity measured at 48 hpe with the indicated constructs. a.u., arbitrary unit; EP, electroporation. Error bars show means ± SEM. **, $P < 0.01$. Bars, 50 µM.

enabled us to calculate the total length of the cell cycle (Tc), which appeared to be significantly shorter after SMAD1/5 inhibition (mean Tc of 12.9 ± 0.9 h for control, 11.3 ± 0.7 h for sh-S1, and 10.8 ± 1.1 h for sh-S5: Fig. 6 F). Calculating the S-phase length (Ts) revealed a marked shortening after *Smad1/5* knockdown (mean Ts of 5.9 ± 0.6 h for control, 3.7 ± 0.4 h for sh-S1, and 3.1 ± 0.5 h for sh-S5; Fig. 6 F).

The length of the G2 phase (TG2) was derived from the BrdU labeling index of the mitotic electroporated cells (GFP$^+$;pH3$^+$) in the VZ at 48 hpe (Fig. 6 C). We observed no obvious changes in the labeling index curves of sh-S1, sh-S5, or control cells (Fig. 6 D), and the mean G2 duration calculated by the paradigm of labeled mitoses method (see Materials and methods; Quastler and Sherman, 1959) was comparable for control (1.3 ± 0.1 h), sh-S1 (1.4 ± 0.1 h), and sh-S5 (1.4 ± 0.1 h) cells (Fig. 6 F).

The duration of the M phase (TM) was derived from the mitotic index of the electroporated cells, and there were no changes in the mitotic indices after electroporation with control or sh-S1/5 vectors (mitotic index 0.04 ± 0.01 for control, 0.05 ± 0.01 for sh-S1, and 0.05 ± 0.01 for sh-S5; Fig. 6 E) or after applying a correction for the slight differences in growth fraction values (corrected mitotic index of 0.05 ± 0.01 for control, 0.07 ± 0.01 for sh-S1, and 0.07 ± 0.01 for sh-S5; Fig. 6 E). The TM was then calculated from the Tc and yielded comparable values for control (0.64 ± 0.1 h), sh-S1 (0.80 ± 0.1 h), and sh-S5 (0.76 ± 0.2 h) cells (Fig. 6 F). Finally, determination of the Tc, Ts, TG2, and TM allowed us to deduce the length of the G1 phase (TG1), which was similar in control (5.0 ± 1.7 h), sh-S1 (5.4 ± 1.3 h), and sh-S5 (5.5 ± 1.9 h) cells (Fig. 6 F). Together, these analyses indicated that interfering

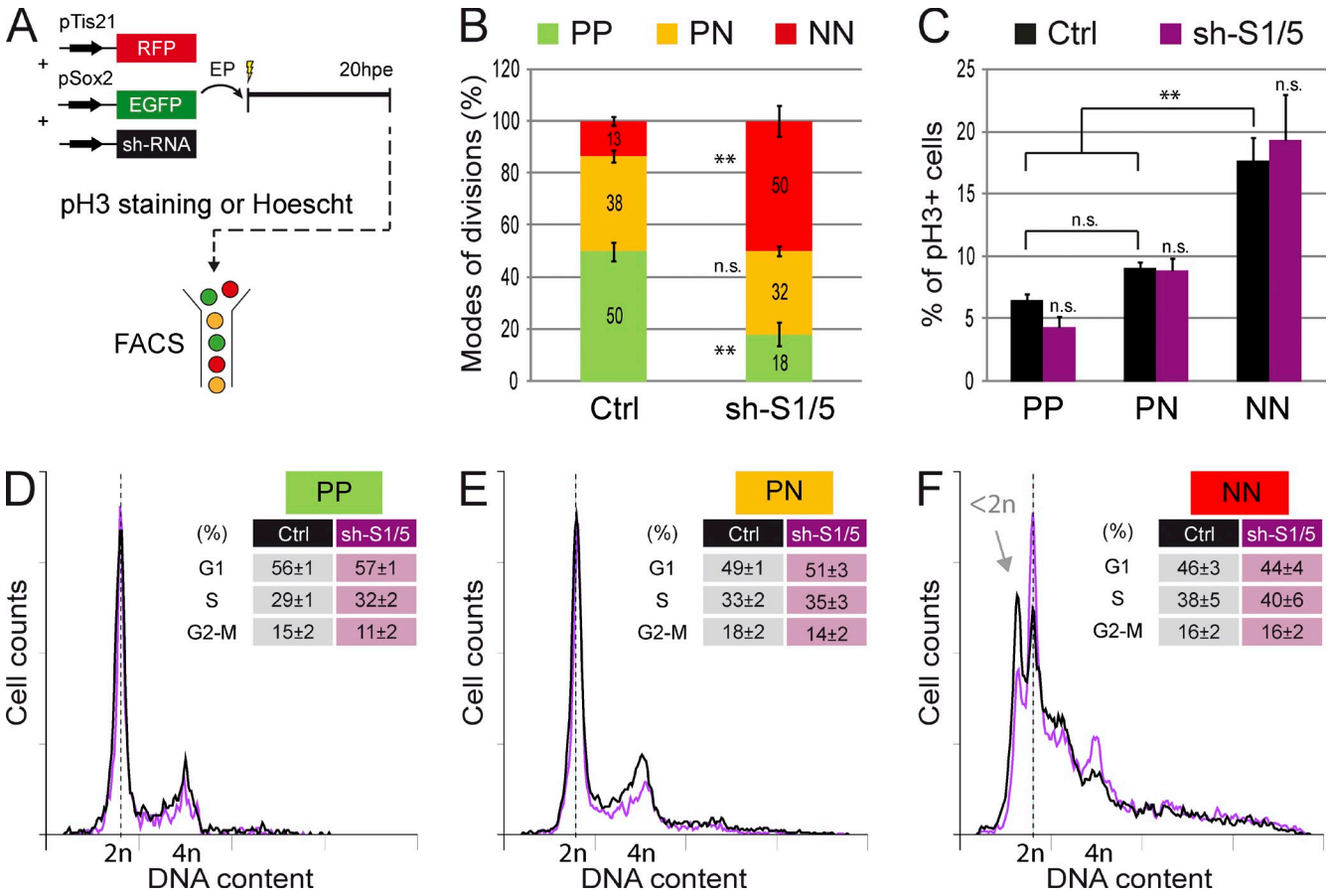

Figure 7. **Analysis of the cell cycle distribution of PP, PN, and NN progenitors.** (A) Illustration of the methodology used to analyze the cell cycle distribution of PP, PN, and NN divisions by flow cytometry in dissociated cells processed for pH3 staining or Hoechst incorporation 20 hpe with pTis21:RFP, pSox2:EGFP, and control or *Smad1/5* shRNA vectors. (B) Percentages of mitotic ($pH3^+$) $GFP^+;RFP^-$ (PP), $GFP^+;RFP^+$ (PN), and $GFP^-;RFP^+$ (NN) cells electroporated with control (Ctrl) or *Smad1/5* shRNA (sh-S1/5). (C) Mitotic indices of $GFP^+;RFP^-$ (PP), $GFP^+;RFP^+$ (PN), and $GFP^-;RFP^+$ (NN) cells electroporated with control or *Smad1/5* shRNA (sh-S1/5). (D–F) Overlays of representative DNA content profiles obtained after Hoechst incorporation for $GFP^+;RFP^-$ (D, PP), $GFP^+;RFP^+$ (E, PN), and $GFP^-;RFP^+$ (F, NN) cells electroporated with control or sh-S1/5 constructs. Mean values of the percentages of cells in G1, S, and G2–M phases are presented. EP, electroporation. Error bars show means ± SEM. **, $P < 0.01$.

with SMAD1/5 activity in spinal progenitors additionally causes a reduction of their mean cell cycle length as a result of a shortening of the S phase.

We also evaluated the mean number of divisions that electroporated cells performed in vivo using the CellTrace violet, a cytoplasmic retention dye, which is specifically subject to dilution upon cell division. The CellTrace violet was injected into the neural tube lumen at the time of electroporation, and its fluorescence intensity was measured in dissociated GFP^+ cells at 48 hpe by flow cytometry (Fig. 6 G). Compared with control embryos, electroporation with sh-S1 or sh-S5 increased the mean CellTrace violet intensity by 41% (mean violet intensity of 6.6 ± 0.5 for control, 9.3 ± 0.8 for sh-S1, and 9.3 ± 0.5 for sh-S5; $P < 0.01$; Fig. 6, H and I), indicating that on average, spinal progenitors with impaired SMAD1/5 activity underwent fewer divisions. Conversely, hyperactivation of SMAD1/5 activity through electroporation of SMAD1-SD and SMAD5-SD caused a reduction in the mean CellTrace violet intensity (mean violet intensity of 7.7 ± 0.6 for control, 5.8 ± 0.4 for SMAD1-SD, and 4.2 ± 0.4 for SMAD5-SD; $P < 0.01$; Fig. 6, J and K), implying that more neural progenitors divided in response to SMAD1/5 overactivation.

The regulation of the modes of division by SMAD1/5 precedes cell cycle alterations

It appears that modulating SMAD1/5 activity within spinal progenitors alters both their mode of division and their cell cycle kinetics. We next established an experimental design to discriminate which of these two events is directly controlled by SMAD1/5. Accordingly, we coelectroporated the two reporters (pTis21:RFP and pSox2:GFP) with the sh-S1/5 or control vectors, and we then dissociated the neural tube cells at 20 hpe, stained them for pH3, and analyzed them by flow cytometry (Fig. 7 A). The assessment of the proportions of PP, PN, and NN divisions among the mitotic ($pH3^+$) electroporated cells confirmed that *Smad1/5* knockdown increased the percentage of NN divisions at the expense of PP ones, without significantly altering PN divisions (Fig. 7 B). In the same set of experiments, we calculated the mitotic index for each of the three progenitor subpopulations. After control electroporation, although the percentages of mitotic PP and PN cells were comparable, that of mitotic NN progenitors was significantly higher (percentages of $pH3^+$ cells were 6.5 ± 0.5 for PP, 9.1 ± 0.4 for PN, and 17.6 ± 1.9 for NN in control conditions; $P < 0.01$; Fig. 7 C), suggesting that NN divisions were faster. Importantly, interfering with

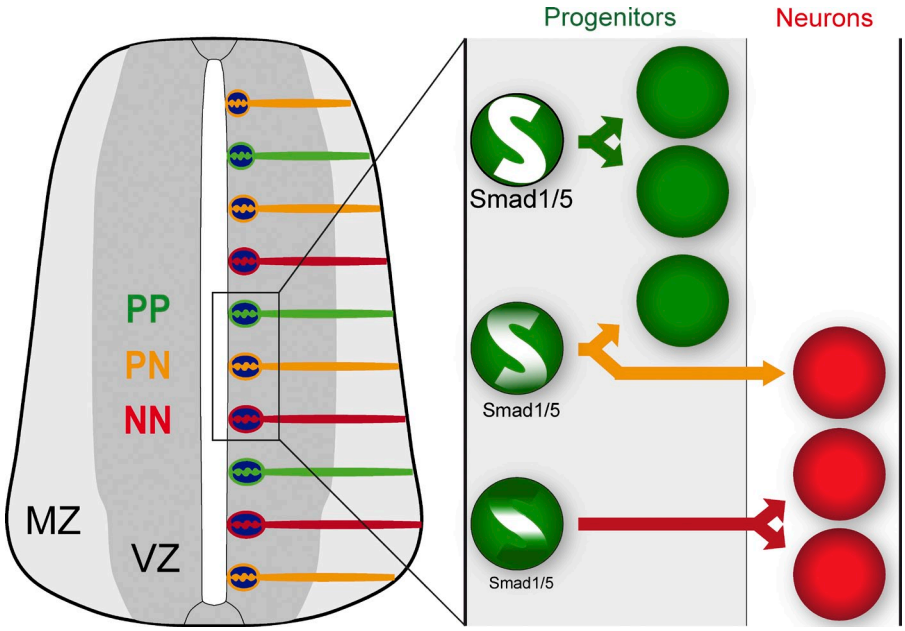

Figure 8. **Model of the control imposed by SMAD1/5 on the mode of divisions of neural progenitors during spinal interneuron generation.** From the onset of spinal interneuron generation, neural progenitors undergo along the dorsal–ventral axis three distinct modes of division: the symmetric proliferative mode (PP, green arrow), which results in the generation of two daughter progenitor cells; the asymmetric mode (PN, yellow arrow), leading to the generation of one daughter progenitor cell while the other daughter cell is committed to differentiate into a neuron; or the symmetric neurogenic (NN, red arrow) mode through which the two daughter cells are committed to differentiation. The decision of a neural progenitor to undergo one division mode or another is under the control of SMAD1/5, so that high, intermediate, and low levels of SMAD1/5 activity dictate neural progenitors to undergo PP, PN, and NN divisions, respectively.

SMAD1/5 activity did not affect the mitotic indices of any of the three progenitor populations compared with their respective controls (percentages of $pH3^+$ cells were 4.3 ± 0.9 for PP, 8.9 ± 1.0 for PN, and 19.3 ± 3.7 for NN after sh-S1/5 electroporation; Fig. 7 C).

Alternatively, the DNA content was assessed by flow cytometry after Hoechst staining, and its profile was similar for PP and PN cells (Figs. 7, D and E; and S4 C). In contrast, the NN cell population presented a surprising DNA content profile, showing numerous peaks and including a nonnegligible proportion of hypoploidy (Figs. 7 F and S4 D). Studying the distribution of the different cell cycle phases of the diploid populations revealed a significantly higher proportion of PP cells in G1 than PN and NN (mean percentages of G1 were 56 ± 1 for PP, 49 ± 1 for PN, and 46 ± 3 for NN; $P < 0.05$; Figs. 7, D–F; and S4 E), whereas the percentages of these diploid cells in S and G2–M were not significantly affected (Fig. 7, D–F). The aneuploid NN subpopulation presented significant alterations in the proportions of cells in the G1, S, and G2–M phases compared with the diploid populations (Fig. S4 E). SMAD1/5 inhibition affected the proportions of total PP, PN, and NN cells in a way similar to that previously observed in the mitotic electroporated cells (compare Fig. S4 B with Fig. 7 B), although it did not significantly alter either the DNA content profile or the cell cycle distribution in any of the cell populations (Figs. 7, D–F; and S4 E).

Therefore, these results confirmed that SMAD1/5 activity regulated the balance between the modes of divisions of spinal progenitors and further suggested that these changes in cell fate preceded the changes in cell cycle kinetics. Altogether, these data imply that SMAD1/5 directly control the mode of division of neural progenitors during spinal interneuron generation.

Discussion

Combining newly developed markers that identify the three modes of progenitor division in the developing spinal cord (self-expanding [PP], self-renewing [PN], and self-consuming [NN]) with in vivo manipulations of SMAD1/5 activity, we identified a new role for the canonical BMP effectors SMAD1/5 in dictating the mode of division of neural progenitors during spinal interneuron generation (Fig. 8). Inhibiting SMAD1/5 activity in spinal progenitors at the onset of interneuron generation provoked a premature increase in NN divisions at the expense of PP ones, leading neural progenitors to prematurely exit the cell cycle and undergo differentiation. A consequence of these cell-autonomous effects would be the depletion of the neural progenitor pool, as reflected by the reduction in the size of the VZ containing $Sox2^+$ neural progenitors. This would explain why we ultimately observed a reduction in neuron number after SMAD1/5 inhibition in the developing spinal cord (this study; Le Dréau et al., 2012). A similar mechanism could account for the impaired neurogenesis reported after BMP signaling inhibition during both corticogenesis and dentate development (Segklia et al., 2012; Choe et al., 2013). Accordingly, the canonical BMP signaling thus appears to be crucial for stem cell maintenance both during neural development and adult neurogenesis (Lim et al., 2000; Mira et al., 2010).

Variations in cell cycle kinetics are correlated with distinct stem cell fates in the developing cerebral cortex (Dehay and Kennedy, 2007; Salomoni and Calegari, 2010). By taking advantage of the pSox2:EGFP and pTis21:RFP reporters, we distinguished between spinal progenitors based on their mode of division and found that the cell cycle parameters differed in these three populations. In particular, there was an approximately twofold increase in the mitotic index of the NN progenitors over that of the PP and PN populations, suggesting that progenitors committed to NN divisions have a shorter cell cycle. This was consistent with the fact that the premature differentiation provoked by SMAD1/5 inhibition was accompanied by a reduction of the mean cell cycle length, the latter was caused by a shortening of the S phase. Thus, S-phase shortening was associated with neuronal commitment in the developing spinal cord,

as reported recently for neural progenitors in the developing mouse cerebral cortex (Arai et al., 2011). Yet our analyses demonstrated that SMAD1/5 inhibition altered the balance between these three division modes without provoking any significant changes in the cell cycle parameters. This leads us to propose that cell fate determination precedes any changes in the cell cycle and that the reduction of the mean cell cycle length is a consequence of the alteration in the balance of the modes of divisions, rather than a cause. Accordingly, differential regulation of cyclin D2 in response to asymmetric divisions was recently demonstrated in the developing murine cerebral cortex, its expression only persisting in the daughter cell that inherited the basal process and that maintained its progenitor identity (Tsunekawa et al., 2012). Importantly, the BMP-induced maintenance of adult stem cells is associated with quiescence (Lim et al., 2000; Mira et al., 2010; Ono et al., 2011; Oshimori and Fuchs, 2012), arguing against the idea that BMP activity determines stem cell fate by stimulating cell cycle progression.

Another significant observation was the identification of aneuploid progenitors in the developing spinal cord. There is a growing body of evidence that aneuploid neurons are generated during cerebral cortex development (Rehen et al., 2001; Peterson et al., 2012) and adult neurogenesis (Rehen et al., 2001; Muotri and Gage, 2006) and that these neurons are functional (Kingsbury et al., 2005). Aneuploidy is thought to represent one of the numerous mechanisms causing the variations in DNA content that occur in the CNS, and it is thought to contribute to neuronal diversity and potentially enhance an organism's adaptability (Kingsbury et al., 2006; Muotri and Gage, 2006). Interestingly, we only detected aneuploidy in the NN progenitors committed to terminal neurogenic divisions. Thus, the generation of aneuploid cells might be facilitated by the shortening of the S phase. In fact, changes in the expression of factors key to cell cycle regulation, DNA replication, DNA repair, and chromatin remodeling have already been observed in a genome-wide expression analysis that compared expanding (pTis21:GFP$^-$) and committed (pTis21:GFP$^+$) neural progenitors in the developing murine cerebral cortex (Arai et al., 2011). Restricting the occurrence of aneuploidy to terminally differentiating neural progenitors might therefore prevent the risk of transmitting potentially deleterious DNA alterations to the whole lineage.

Both the quantification of endogenous pS158 intensity and the comparison of *Id* gene expression levels in the three different progenitor subpopulations supported the notion that the mode of division was dictated by an endogenous gradient of SMAD1/5 activity during spinal interneuron generation, with the weakest activity forcing neural progenitors to enter NN divisions (Fig. 8). The idea of a gradient of BMP activity acting as a fate determinant was proposed recently in *Drosophila* germline stem cells (Xia et al., 2012), leading to the intriguing hypothesis that dramatic cellular decisions such as stem cell fate originate from subtle variations in the levels of SMAD activity. We quantified levels of SMAD1/5 activity during mitosis; however, we do not exclude the possibility that regulating cell fate decision through modifications of SMAD1/5 activity could occur earlier in the cell cycle. Another interesting question will be to determine whether *Id2* and *Id3* are effectively involved in instructing the mode of spinal progenitor division, as suggested by their expression gradually decreasing in PP, PN, and NN progenitors.

The canonical BMP activity is highly dynamic both spatially and temporally during spinal cord development (Le Dréau et al., 2012; Le Dréau and Martí, 2013; Tozer et al., 2013). The activity of the canonical BMP pathway is restricted to the most dorsal part of the neural tube at early stages (Le Dréau et al., 2012; Tozer et al., 2013) but deploys along the whole dorsal–ventral axis at the onset of interneuron generation (Le Dréau et al., 2012). Thus, the canonical BMP activity is likely to be required for the maintenance of self-expanding divisions only from that stage. Accordingly, Sonic Hedgehog signaling is crucial for the maintenance of self-expanding divisions earlier during development, within the context of motor neuron generation (Saade et al., 2013). Together, these results support the notion that the influence of a particular extrinsic factor on neural stem and progenitor cells is both stage and area specific (Falk and Sommer, 2009). Considering the diversity of extrinsic signals reported to affect neural stem cell maintenance (Fuentealba et al., 2012; Tiberi et al., 2012; Franco and Müller, 2013), one of the future challenges in the field of stem cell biology will be to identify the molecular mechanisms underlining these context-specific effects and to uncover the common key intrinsic factors acting downstream of these extrinsic cues to command the mode of stem cell division.

Materials and methods

Chick embryos

Eggs from white Leghorn chickens were staged according to the method of Hamburger and Hamilton (1951). In ovo electroporation was performed at stage HH14 (54 h of incubation with 22 somites) unless otherwise notified, and the embryos were recovered at the times indicated (12–72 hpe). Electroporation was performed as described previously (Le Dréau et al., 2012).

DNA constructs

The pCAGGS_ires_H2B-RFP and pCS2:H2B-GFP vectors were used at a concentration of 0.5 µg/µl as controls for electroporation. Inhibition of endogenous SMAD1/5 activity was induced by electroporation of pSuper or pSHIN vectors (3–4 µg/µl), which produce shRNAs that specifically target chick *Smad1* and *Smad5* and reduce to ~50% of their endogenous mRNA levels (Le Dréau et al., 2012). Alternatively, inhibition of SMAD activity was achieved by overexpressing the dominant-negative *Smad5* mutant Somitabun (Le Dréau et al., 2012) at various concentrations (combinations of 0:2, 0.5:1.5, 1:1, and 2:0 µg/µl of pCS2/Somitabun and empty pCS2 constructs]. The SMAD1-SD and SMAD5-SD mutants were used to overactivate endogenous SMAD1/5 activity. As previously described (Le Dréau et al., 2012), these pseudophosphorylated mutant versions of SMAD1 and SMAD5 were generated by PCR-mediated site-directed mutagenesis, replacing the three serines at the C-terminal end by aspartic acid, and cloned into pCAGGS-ires-GFP or into pCAGGS-ires-H2B-RFP.

The pTis21:RFP reporter was created by inserting a fragment of the promoter of the mouse *Tis21* gene (−442 to 65) into the ptk:RFP plasmid (Uchikawa et al., 2003), amplified from the mouse genome by PCR using the primers 5′-GGGATGAGTGGCAGAGATGT-3′ and 5′-GGTGGCTGAGGAAGTAGCTG-3′. The pSox2:EGFP reporter consisted of an EGFP cassette from the ptk2:EGFP plasmid under the control of a fragment of the chicken *Sox2* promoter covering the 7.6–14 kb of the *Sox2* locus. This fragment (provided by M. Uchikawa, Osaka University, Osaka, Japan) has already been shown to specifically reproduce endogenous Sox2 promoter activity in the developing spinal cord (Uchikawa et al., 2003).

The endogenous activities of the Sonic Hedgehog and canonical Wnt pathways were assessed using reporter constructs producing H2B-RFP under the control of a promoter containing synthetic 8× 3′GBSs (Sasaki et al., 1997; Saade et al., 2013) or synthetic T cell factor binding sites

(Korinek et al., 1998), respectively. As previously described (Le Dréau et al., 2012), the BRE:GFP reporter consists of an artificial promoter containing two copies of two distinct, highly conserved BRE encompassing the genomic regions −1,032/−1,052 (SBE-3, SBE-2, and GC′-5) and −1,080/−1,105 (CAGC-2, CAGC-1, and GC′-3,4) of the natural human *Id1* promoter (Korchynskyi and ten Dijke, 2002), which has been cloned upstream of the herpes simplex virus thymidine kinase minimal promoter in a vector carrying EGFP.

The Tubb3enh:EGFP reporter (Bergsland et al., 2011), consisting of an enhancer of the mouse Tubb3 gene inserted into the multiple cloning site of the bGlobin-GFP-MCSIII vector, was provided by J. Muhr (Karolinska Institute, Stockholm, Sweden) . The mPlum construct, which was developed and provided by the R.Y. Tsien laboratory (Howard Hughes Medical Institute, University of California, San Diego, La Jolla, CA), produces from a pUC19 backbone a far-red–emitting fluorescent protein obtained by directed mutagenesis of a monomeric mutant of DsRed (Wang and Tsien, 2006).

Immunohistochemistry and microscopy

Embryos were fixed for 2 h at 4°C in 4% PFA, and immunostaining was performed on either vibratome (40 µm) or cryostat (16 µm) sections following standard procedures. For BrdU detection, sections were incubated in 2 N HCl for 30 min and then rinsed with 0.1 M $Na_2B_4O_7$, pH 8.5. After washing in PBS–0.1% Triton X-100, the sections were incubated with the appropriate primary antibodies: rabbit anti-GFP, rabbit anti-Sox2, mouse anti-HuC/D, and mouse anti–lamin B1 (Invitrogen), rat anti-BrdU (AbD Serotec), rabbit anti-pS158 (Cell Signaling Technology), or rabbit anti-pH3 (EMD Millipore). Alexa Fluor 488–, Alexa Fluor 555–, and Cy5-conjugated secondary antibodies were obtained from Invitrogen and Jackson ImmunoResearch Laboratories, Inc. Sections were stained with 1 µg/ml DAPI and mounted in Mowiol (Sigma-Aldrich). Images were acquired at room temperature with the LAS software (Leica) on a confocal microscope (SP5; Leica) using 20× (dry HC Plan Apochromat, NA 0.70), 40× (oil HCX Plan Apochromat, NA 1.25–0.75), or 63× (oil HCX Plan Apochromat, NA 1.40–0.60) objective lenses. Maximal projections obtained from 2-µm z-stack images were processed in Photoshop CS5 and Illustrator CS4 (Adobe) for image merging and resizing and cell counting. Cell counts were typically performed on three to five images per embryo. The data represent the means ± SEM obtained from the values of at least $n = 5$ different embryos, for each time point and experimental condition.

Measurement of the Sox2$^+$ (VZ) and HuC/D$^+$ (MZ) areas

The effects of SMAD1/5 inhibition on the total numbers of neural progenitors or neurons were assessed by measuring the area occupied, respectively, by the VZ (containing the Sox2$^+$ progenitors) or the MZ (formed by the HuC/D$^+$ neurons). These areas were obtained from pictures of chick neural tube transverse sections stained for Sox2 and HuC/D, 48 hpe. The Sox2 and HuC/D channels were then extracted and measured using the ImageJ software (National Institutes of Health) by adapting the methodology previously described by K. Straatman (Advanced Imaging Facilities, University of Leicester, Leicester, England, UK). In brief, after splitting the channels of 2-µm z-stack maximal projection images, the look-up table of the channel of interest was inverted, and its threshold was adjusted. The HuC/D$^+$ or Sox2$^+$ areas were then measured for both control and electroporated neural tube sides by a particle analysis using a pixel^2 size ranging from 1,000 to infinity. The data are presented as the ratios ± SEM obtained by standardizing the values of the electroporated side to the corresponding values of the respective nonelectroporated side. Three images were used to calculate a mean value per embryo. The data represent the means ± SEM obtained from the values of ≥10 different embryos per experimental condition.

Quantification of pS158 staining

The intensity of the pS158 staining was quantified within mitotic progenitors during the distinct modes of divisions. HH14 embryos electroporated with either pSox2:EGFP and a control H2B-RFP vector, pTis21:RFP and a control H2B-GFP vector, or pSox2:EGFP and pTis21:RFP were recovered at 24 hpe and processed for immunohistochemistry using the phospho-SMAD1/5/8 antibody (pS158; Cell Signaling Technology). Maximal projections obtained from 2-µm z-stack images taken with a confocal microscope (SP5) were then analyzed using the ImageJ software. The nuclear area of the electroporated mitotic progenitors was then delimitated by polygonal selection, and the mean intensity of the nuclear pS158 staining was quantified as the mean gray value. Quantifications were performed on five to nine different images to calculate a mean value per embryo. The data represent the means ± SEM obtained from the values of at least eight different embryos per experimental condition.

Flow cytometry

HH14 embryos were recovered 16 or 20 h after coelectroporation with the pSox2:EGFP and pTis21:RFP reporters, in the absence (for PCR analysis) or additional presence (for cell cycle analysis) of control or sh-S1/5 vectors. Cell suspensions were obtained from pools of six to eight dissected neural tubes after digestion with trypsin-EDTA (Sigma-Aldrich) for 10–15 min and further processed on a cell sorter (FACS Aria III; BD) for EGFP and RFP fluorescence. To analyze the DNA content, the samples were incubated with 10 µg/ml of Hoechst (Sigma-Aldrich) at 37°C for 30 min. The cellular DNA content was analyzed in single fluorescence histograms using the Multicycle software (Phoenix Flow Systems). The mean ± SEM represents the percentages of cells in G1, S, and G2–M from the analysis of 9–10 cell pools per experimental condition. At least 5,000 cells for each progenitor population (PP, PN, and NN) were analyzed per pool. Alternatively, dissociated cell pools were processed for pH3 immunocytochemistry and analyzed for EGFP, RFP, and Cy5 fluorescence. The data are presented as the means ± SEM obtained from four to five cell pools per experimental condition.

Real-time PCR

Total RNA extracts were obtained following the TRIZOL protocol (Invitrogen) from subpopulations of GFP$^+$;RFP$^-$ (PP), GFP$^+$;RFP$^+$ (PN), and GFP$^-$;RFP$^+$ (NN) cells segregated and purified by FACS (20,000 cells per pool). Reverse transcription and real-time PCR were performed according to manufacturer's instructions (Roche) using a lightcycler (LC 480; Roche). Specific primers used for quantitative PCR amplification of *Id* genes were purchased (QuantiTect Primer Assays; QIAGEN). Oligonucleotides specific for chick Gapdh were used for normalization. PCR amplifications were assessed from four independent cell pools per experimental condition. Data are expressed in arbitrary units and represent mean standardized values ± SEM.

Analysis of the mean number of divisions

We assessed the mean number of divisions of neural progenitors in vivo using the cell proliferation kit (CellTrace violet; Invitrogen). Here, the violet cell tracer (1 mM), a cytoplasmic retention dye that becomes diluted as cells divide, was injected into the neural tube lumen at the time of electroporation. HH14 embryos were recovered at 48 hpe, the neural tube was carefully removed, and the cells were dissociated after a 10–15-min digestion in trypsin-EDTA. The fluorescence intensity of the violet tracer was measured in viable dissociated electroporated GFP$^+$ cells in the 405/450-nm excitation/emission range on a flow cytometer (Gallios; Beckman Coulter). The data are presented as the mean CellTrace violet intensity (±SEM) obtained from 6–16 embryos per experimental condition.

In situ hybridization

HH14 embryos were recovered at 24 hpe, fixed overnight at 4°C in 4% PFA, rinsed in PBS, and processed for whole-mount RNA in situ hybridization following standard procedures using probes for chick *Id1*, *Id2*, *Id3*, and *Id4* (from the chicken EST project; UK Human Genome Mapping Project Resource Centre). Hybridized embryos were postfixed in 4% PFA and washed in PBT (PBS with Tween). 45-µM-thick sections were cut with a vibratome (VT1000S; Leica), mounted, and photographed using a microscope (DC300; Leica). The data show representative pictures obtained from three independent embryos per experimental condition.

Luciferase reporter assay

Transcriptional activity of the *NeuroD* promoter was assessed in vivo following electroporation of the pNeuroD:Luc vector and a renilla luciferase reporter construct carrying the cytomegalovirus immediate early enhancer promoter for normalization (Promega), together with the indicated DNAs. 24 hpe, the neural tubes were dissected and processed following the Dual Luciferase Reporter Assay System protocol (Promega), as described previously (Le Dréau et al., 2012). The data are presented as the means ± SEM from 11–12 embryos per experimental condition.

Calculation of the duration of the cell cycle phases

The lengths of the cell cycle (Tc) and S phase (Ts) were calculated from the BrdU labeling indices assessed for electroporated cells (H2B-RFP$^+$) located in the VZ at 48 hpe, which were obtained from cumulative BrdU experiments following the nonlinear regression method described by Nowakowski et al. (1989). In brief, the best nonlinear parameters fitting the experimental data allow the calculation of the duration needed for the BrdU labeling index to reach the plateau, which provides the length Tc − Ts; the fraction of maximum labeling index, which corresponds to the growth

fraction value (GF); and the intercept of the BrdU labeling curve with the *y* axis, representing the fraction of cycling cells in S phase [GF × (Ts/Tc)].

The TM was derived from the mitotic index (MI) and calculated from the respective Tc, so that TM = Tc × MI, as reported previously (Arai et al., 2011). A correction was applied to the values obtained from cell counts, to take into account the slight differences in the growth fraction (deduced from the cumulative BrdU experiments): corrected TM = Tc × MI/GF.

The TG2 was calculated using the mitotic labeling index data obtained from cumulative BrdU experiments, according to the percentage of labeled mitoses paradigm as previously described (Quastler and Sherman, 1959; Peco et al., 2012), so that the mean TG2 length corresponds to the duration of BrdU incorporation required to obtain the half-maximal appearance of GFP^+;$pH3^+$:$BrdU^+$ cells. By means of an error minimization algorithm, provided by J. Buceta (Parc Cientific de Barcelona, Barcelona, Spain), the mitotic labeling index data were fitted to the following function:

$$f(t) = \frac{(t / T_{G2})^n}{1 + (t / T_{G2})^n}.$$

In this function, there are two fitting parameters, T_{G2} and n, which correspond, respectively, to TG2 and to the sharpness of the mitotic response. Note that $f(T_{G2}) = 1/2$ regardless the value of n.

The errors of the mean Tc, Ts, TM, TG2, and TG1 were estimated using the standard error propagation technique using the corresponding formulas. In brief, given a set of points $(x_i, y_i \pm \sigma_i)$, in which i = 1, 2, . . ., *M*, and a nonlinear fitting function $Y(x; \{a\})$, in which $\{a\}$ stands for a set of *N* parameters $(a_1, a_2, \ldots, a_N)$, the error minimization algorithm implements a standard Newton scheme to find the set $\{a\}$ that minimizes the amount:

$$\sum_{i=1}^{M} \left(\frac{Y(x_i; \{a\}) - y_i}{\sigma_i} \right)^2.$$

Thus, we weight differently every experimental point depending on its error (the larger the error, the smaller its weight).

Statistical analysis

The quantitative data are expressed as means ± SEM. Statistical analysis was performed using the StatView software (SAS Institute Inc.), and significance was assessed by performing analysis of variance followed by the Student–Newman–Keuls test. Otherwise, the significance was assessed using the Student's *t* test (Figs. 2, D and F; and 7, B–F). Concerning the durations of the cell cycle phases (Fig. 6) and the extrapolation of the proportion of PN (Figs. 3, E and F; and 4 C), the errors were estimated using the standard error propagation technique using the corresponding formulas (*, P < 0.05; **, P < 0.01; and ***, P < 0.001).

Online supplemental material

Fig. S1 shows the analysis of the mRNA expression of *Id* genes in response to modulations of the canonical BMP activity. Fig. S2 presents the proportions of $pTis21^+$ and $pSox2^+$ divisions obtained in response to experiments of rescue and dose-dependent effects of SMAD1/5 inhibition. Fig. S3 shows representative pictures of the cell-autonomous and overall effects of SMAD1/5 inhibition on the neuronal differentiation of spinal progenitors. Fig. S4 gives further details on the flow cytometry analysis of the cell cycle distribution of the PP, PN, and NN progenitors. Online supplemental material is available at http://www.jcb.org/cgi/content/full/jcb.201307031/DC1.

The authors wish to thank Susana Usieto for her invaluable technical assistance and members of E. Martí's laboratory for their helpful comments. We thank Dr. Masanori Uchikawa, Dr. Jonas Muhr, and Dr. Roger Tsien for kindly providing DNAs as well as Dr. Javier Buceta (Computer Simulation and Modelling Laboratory) for thoughtful discussions and providing the error minimization algorithm.

The work in E. Martí's laboratory was supported by the grants BFU2010-18959 and CSD2007-00008.

The authors declare no competing financial interests.

Submitted: 4 July 2013
Accepted: 13 December 2013

References

Alarcón, C., A.I. Zaromytidou, Q. Xi, S. Gao, J. Yu, S. Fujisawa, A. Barlas, A.N. Miller, K. Manova-Todorova, M.J. Macias, et al. 2009. Nuclear CDKs drive Smad transcriptional activation and turnover in BMP and TGF-beta pathways. *Cell*. 139:757–769. http://dx.doi.org/10.1016/j.cell.2009.09.035

Arai, Y., J.N. Pulvers, C. Haffner, B. Schilling, I. Nüsslein, F. Calegari, and W.B. Huttner. 2011. Neural stem and progenitor cells shorten S-phase on commitment to neuron production. *Nat. Commun*. 2:154. http://dx.doi.org/10.1038/ncomms1155

Bergsland, M., D. Ramsköld, C. Zaouter, S. Klum, R. Sandberg, and J. Muhr. 2011. Sequentially acting Sox transcription factors in neural lineage development. *Genes Dev*. 25:2453–2464. http://dx.doi.org/10.1101/gad.176008.111

Choe, Y., A. Kozlova, D. Graf, and S.J. Pleasure. 2013. Bone morphogenic protein signaling is a major determinant of dentate development. *J. Neurosci.* 33:6766–6775. http://dx.doi.org/10.1523/JNEUROSCI.0128-13.2013

Das, R.M., and K.G. Storey. 2012. Mitotic spindle orientation can direct cell fate and bias Notch activity in chick neural tube. *EMBO Rep.* 13:448–454. http://dx.doi.org/10.1038/embor.2012.42

Dehay, C., and H. Kennedy. 2007. Cell-cycle control and cortical development. *Nat. Rev. Neurosci.* 8:438–450. http://dx.doi.org/10.1038/nrn2097

Falk, S., and L. Sommer. 2009. Stage- and area-specific control of stem cells in the developing nervous system. *Curr. Opin. Genet. Dev*. 19:454–460. http://dx.doi.org/10.1016/j.gde.2009.08.002

Franco, S.J., and U. Müller. 2013. Shaping our minds: stem and progenitor cell diversity in the mammalian neocortex. *Neuron*. 77:19–34. http://dx.doi.org/10.1016/j.neuron.2012.12.022

Fuentealba, L.C., K. Obernier, and A. Alvarez-Buylla. 2012. Adult neural stem cells bridge their niche. *Cell Stem Cell*. 10:698–708. http://dx.doi.org/10.1016/j.stem.2012.05.012

Ghosh, S., T. Marquardt, J.P. Thaler, N. Carter, S.E. Andrews, S.L. Pfaff, and T. Hunter. 2008. Instructive role of aPKCzeta subcellular localization in the assembly of adherens junctions in neural progenitors. *Proc. Natl. Acad. Sci. USA*. 105:335–340. http://dx.doi.org/10.1073/pnas.0705713105

Gonzalez, C. 2007. Spindle orientation, asymmetric division and tumour suppression in *Drosophila* stem cells. *Nat. Rev. Genet.* 8:462–472. http://dx.doi.org/10.1038/nrg2103

Göritz, C., and J. Frisén. 2012. Neural stem cells and neurogenesis in the adult. *Cell Stem Cell*. 10:657–659. http://dx.doi.org/10.1016/j.stem.2012.04.005

Götz, M., and W.B. Huttner. 2005. The cell biology of neurogenesis. *Nat. Rev. Mol. Cell Biol.* 6:777–788. http://dx.doi.org/10.1038/nrm1739

Hamburger, V., and H.L. Hamilton. 1951. A series of normal stages in the development of chick embryo. *J. Morphol.* 88:49–92. http://dx.doi.org/10.1002/jmor.1050880104

Hild, M., A. Dick, G.J. Rauch, A. Meier, T. Bouwmeester, P. Haffter, and M. Hammerschmidt. 1999. The smad5 mutation somitabun blocks Bmp2b signaling during early dorsoventral patterning of the zebrafish embryo. *Development*. 126:2149–2159.

Hollnagel, A., V. Oehlmann, J. Heymer, U. Rüther, and A. Nordheim. 1999. Id genes are direct targets of bone morphogenetic protein induction in embryonic stem cells. *J. Biol. Chem.* 274:19838–19845. http://dx.doi.org/10.1074/jbc.274.28.19838

Kingsbury, M.A., B. Friedman, M.J. McConnell, S.K. Rehen, A.H. Yang, D. Kaushal, and J. Chun. 2005. Aneuploid neurons are functionally active and integrated into brain circuitry. *Proc. Natl. Acad. Sci. USA*. 102:6143–6147. http://dx.doi.org/10.1073/pnas.0408171102

Kingsbury, M.A., Y.C. Yung, S.E. Peterson, J.W. Westra, and J. Chun. 2006. Aneuploidy in the normal and diseased brain. *Cell. Mol. Life Sci.* 63:2626–2641. http://dx.doi.org/10.1007/s00018-006-6169-5

Korchynskyi, O., and P. ten Dijke. 2002. Identification and functional characterization of distinct critically important bone morphogenetic protein-specific response elements in the Id1 promoter. *J. Biol. Chem*. 277:4883–4891. http://dx.doi.org/10.1074/jbc.M111023200

Korinek, V., N. Barker, K. Willert, M. Molenaar, J. Roose, G. Wagenaar, M. Markman, W. Lamers, O. Destree, and H. Clevers. 1998. Two members of the Tcf family implicated in Wnt/β-catenin signaling during embryogenesis in the mouse. *Mol. Cell. Biol.* 18:1248–1256.

Le Dréau, G., and E. Martí. 2012. Dorsal-ventral patterning of the neural tube: a tale of three signals. *Dev. Neurobiol.* 72:1471–1481. http://dx.doi.org/10.1002/dneu.22015

Le Dréau, G., and E. Martí. 2013. The multiple activities of BMPs during spinal cord development. *Cell. Mol. Life Sci.* 70:4293–4305. http://dx.doi.org/10.1007/s00018-013-1354-9

Le Dréau, G., L. Garcia-Campmany, M.A. Rabadán, T. Ferronha, S. Tozer, J. Briscoe, and E. Martí. 2012. Canonical BMP7 activity is required for

the generation of discrete neuronal populations in the dorsal spinal cord. *Development*. 139:259–268. http://dx.doi.org/10.1242/dev.074948

Lesage, B., I. Gutierrez, E. Martí, and C. Gonzalez. 2010. Neural stem cells: the need for a proper orientation. *Curr. Opin. Genet. Dev.* 20:438–442. http://dx.doi.org/10.1016/j.gde.2010.04.013

Lim, D.A., A.D. Tramontin, J.M. Trevejo, D.G. Herrera, J.M. García-Verdugo, and A. Alvarez-Buylla. 2000. Noggin antagonizes BMP signaling to create a niche for adult neurogenesis. *Neuron*. 28:713–726. http://dx.doi.org/10.1016/S0896-6273(00)00148-3

Lui, J.H., D.V. Hansen, and A.R. Kriegstein. 2011. Development and evolution of the human neocortex. *Cell*. 146:18–36. http://dx.doi.org/10.1016/j.cell.2011.06.030

Marthiens, V., and C. ffrench-Constant. 2009. Adherens junction domains are split by asymmetric division of embryonic neural stem cells. *EMBO Rep.* 10:515–520. http://dx.doi.org/10.1038/embor.2009.36

Massagué, J., J. Seoane, and D. Wotton. 2005. Smad transcription factors. *Genes Dev.* 19:2783–2810. http://dx.doi.org/10.1101/gad.1350705

Mira, H., Z. Andreu, H. Suh, D.C. Lie, S. Jessberger, A. Consiglio, J. San Emeterio, R. Hortigüela, M.A. Marqués-Torrejón, K. Nakashima, et al. 2010. Signaling through BMPR-IA regulates quiescence and long-term activity of neural stem cells in the adult hippocampus. *Cell Stem Cell*. 7:78–89. http://dx.doi.org/10.1016/j.stem.2010.04.016

Morin, X., F. Jaouen, and P. Durbec. 2007. Control of planar divisions by the G-protein regulator LGN maintains progenitors in the chick neuroepithelium. *Nat. Neurosci.* 10:1440–1448. http://dx.doi.org/10.1038/nn1984

Morrison, S.J., and A.C. Spradling. 2008. Stem cells and niches: mechanisms that promote stem cell maintenance throughout life. *Cell*. 132:598–611. http://dx.doi.org/10.1016/j.cell.2008.01.038

Müller, T., K. Anlag, H. Wildner, S. Britsch, M. Treier, and C. Birchmeier. 2005. The bHLH factor Olig3 coordinates the specification of dorsal neurons in the spinal cord. *Genes Dev.* 19:733–743. http://dx.doi.org/10.1101/gad.326105

Muotri, A.R., and F.H. Gage. 2006. Generation of neuronal variability and complexity. *Nature*. 441:1087–1093. http://dx.doi.org/10.1038/nature04959

Nowakowski, R.S., S.B. Lewin, and M.W. Miller. 1989. Bromodeoxyuridine immunohistochemical determination of the lengths of the cell cycle and the DNA-synthetic phase for an anatomically defined population. *J. Neurocytol.* 18:311–318. http://dx.doi.org/10.1007/BF01190834

Ono, Y., F. Calhabeu, J.E. Morgan, T. Katagiri, H. Amthor, and P.S. Zammit. 2011. BMP signalling permits population expansion by preventing premature myogenic differentiation in muscle satellite cells. *Cell Death Differ.* 18:222–234. http://dx.doi.org/10.1038/cdd.2010.95

Oshimori, N., and E. Fuchs. 2012. Paracrine TGF-β signaling counterbalances BMP-mediated repression in hair follicle stem cell activation. *Cell Stem Cell*. 10:63–75. http://dx.doi.org/10.1016/j.stem.2011.11.005

Peco, E., T. Escude, E. Agius, V. Sabado, F. Medevielle, B. Ducommun, and F. Pituello. 2012. The CDC25B phosphatase shortens the G2 phase of neural progenitors and promotes efficient neuron production. *Development*. 139:1095–1104. http://dx.doi.org/10.1242/dev.068569

Peterson, S.E., A.H. Yang, D.M. Bushman, J.W. Westra, Y.C. Yung, S. Barral, T. Mutoh, S.K. Rehen, and J. Chun. 2012. Aneuploid cells are differentially susceptible to caspase-mediated death during embryonic cerebral cortical development. *J. Neurosci.* 32:16213–16222. http://dx.doi.org/10.1523/JNEUROSCI.3706-12.2012

Quastler, H., and F.G. Sherman. 1959. Cell population kinetics in the intestinal epithelium of the mouse. *Exp. Cell Res.* 17:420–438. http://dx.doi.org/10.1016/0014-4827(59)90063-1

Rebollo, E., P. Sampaio, J. Januschke, S. Llamazares, H. Varmark, and C. González. 2007. Functionally unequal centrosomes drive spindle orientation in asymmetrically dividing *Drosophila* neural stem cells. *Dev. Cell*. 12:467–474. http://dx.doi.org/10.1016/j.devcel.2007.01.021

Rehen, S.K., M.J. McConnell, D. Kaushal, M.A. Kingsbury, A.H. Yang, and J. Chun. 2001. Chromosomal variation in neurons of the developing and adult mammalian nervous system. *Proc. Natl. Acad. Sci. USA*. 98:13361–13366. http://dx.doi.org/10.1073/pnas.231487398

Saade, M., I. Gutiérrez-Vallejo, G. Le Dréau, M.A. Rabadán, D.G. Miguez, J. Buceta, and E. Martí. 2013. Sonic hedgehog signaling switches the mode of division in the developing nervous system. *Cell Rep*. 4:492–503. http://dx.doi.org/10.1016/j.celrep.2013.06.038

Salomoni, P., and F. Calegari. 2010. Cell cycle control of mammalian neural stem cells: putting a speed limit on G1. *Trends Cell Biol.* 20:233–243. http://dx.doi.org/10.1016/j.tcb.2010.01.006

Sasaki, H., C. Hui, M. Nakafuku, and H. Kondoh. 1997. A binding site for Gli proteins is essential for HNF-3beta floor plate enhancer activity in transgenics and can respond to Shh in vitro. *Development*. 124:1313–1322.

Segklia, A., E. Seuntjens, M. Elkouris, S. Tsalavos, E. Stappers, T.A. Mitsiadis, D. Huylebroeck, E. Remboutsika, and D. Graf. 2012. Bmp7 regulates the survival, proliferation, and neurogenic properties of neural progenitor cells during corticogenesis in the mouse. *PLoS ONE*. 7:e34088. http://dx.doi.org/10.1371/journal.pone.0034088

Shitamukai, A., D. Konno, and F. Matsuzaki. 2011. Oblique radial glial divisions in the developing mouse neocortex induce self-renewing progenitors outside the germinal zone that resemble primate outer subventricular zone progenitors. *J. Neurosci.* 31:3683–3695. http://dx.doi.org/10.1523/JNEUROSCI.4773-10.2011

Suh, H., W. Deng, and F.H. Gage. 2009. Signaling in adult neurogenesis. *Annu. Rev. Cell Dev. Biol.* 25:253–275. http://dx.doi.org/10.1146/annurev.cellbio.042308.113256

Tiberi, L., P. Vanderhaeghen, and J. van den Ameele. 2012. Cortical neurogenesis and morphogens: diversity of cues, sources and functions. *Curr. Opin. Cell Biol.* 24:269–276. http://dx.doi.org/10.1016/j.ceb.2012.01.010

Tozer, S., G. Le Dréau, E. Marti, and J. Briscoe. 2013. Temporal control of BMP signalling determines neuronal subtype identity in the dorsal neural tube. *Development*. 140:1467–1474. http://dx.doi.org/10.1242/dev.090118

Tsunekawa, Y., J.M. Britto, M. Takahashi, F. Polleux, S.S. Tan, and N. Osumi. 2012. Cyclin D2 in the basal process of neural progenitors is linked to non-equivalent cell fates. *EMBO J.* 31:1879–1892. http://dx.doi.org/10.1038/emboj.2012.43

Uchikawa, M., Y. Ishida, T. Takemoto, Y. Kamachi, and H. Kondoh. 2003. Functional analysis of chicken Sox2 enhancers highlights an array of diverse regulatory elements that are conserved in mammals. *Dev. Cell*. 4:509–519. http://dx.doi.org/10.1016/S1534-5807(03)00088-1

Ulloa, F., and J. Briscoe. 2007. Morphogens and the control of cell proliferation and patterning in the spinal cord. *Cell Cycle*. 6:2640–2649. http://dx.doi.org/10.4161/cc.6.21.4822

Wang, L., and R.Y. Tsien. 2006. Evolving proteins in mammalian cells using somatic hypermutation. *Nat. Protoc.* 1:1346–1350. http://dx.doi.org/10.1038/nprot.2006.243

Wang, X., J.W. Tsai, J.H. Imai, W.N. Lian, R.B. Vallee, and S.H. Shi. 2009. Asymmetric centrosome inheritance maintains neural progenitors in the neocortex. *Nature*. 461:947–955. http://dx.doi.org/10.1038/nature08435

Xia, L., X. Zheng, W. Zheng, G. Zhang, H. Wang, Y. Tao, and D. Chen. 2012. The niche-dependent feedback loop generates a BMP activity gradient to determine the germline stem cell fate. *Curr. Biol.* 22:515–521. http://dx.doi.org/10.1016/j.cub.2012.01.056

Ying, Q.L., J. Nichols, I. Chambers, and A. Smith. 2003. BMP induction of Id proteins suppresses differentiation and sustains embryonic stem cell self-renewal in collaboration with STAT3. *Cell*. 115:281–292. http://dx.doi.org/10.1016/S0092-8674(03)00847-X

Yu, F., C.T. Kuo, and Y.N. Jan. 2006. *Drosophila* neuroblast asymmetric cell division: recent advances and implications for stem cell biology. *Neuron*. 51:13–20. http://dx.doi.org/10.1016/j.neuron.2006.06.016